Atomic, Molecular and PAH Emission in Star Formation Regions

B.G. Anandarao

Physical Research Laboratory
Ahmedabad – 380009
India

IDMC – November 22-25, 2011, IUCAA, Pune

Introduction

Herbig Haro Flows in atomic/ionic transitions (Bachiller 1996; Reipurth & Bally 2001)

Molecular Flows (Churchwell 2003)

PAH Emission (Tielens 2008)

Conclusions

The Sites:

Pre-Main-Sequence stars of all masses with jets or outflows

Local shocked ISM through expanding UC/C HII regions created by massive Pre-Main-Sequence stars

The Features:

Forbidden and allowed transitions in atomic and ionic species (e.g., Bachiller 1996; Reipurth & Bally 2001)

CO and other molecular outflows from massive YSOs detected in mm line emission (e.g., Churchwell 2003)

Molecular Hydrogen rotational vibrational emissions in infrared from jets and accretion disks of YSOs (e.g., Watson etal 2010)

M8 – Expansion of HII region

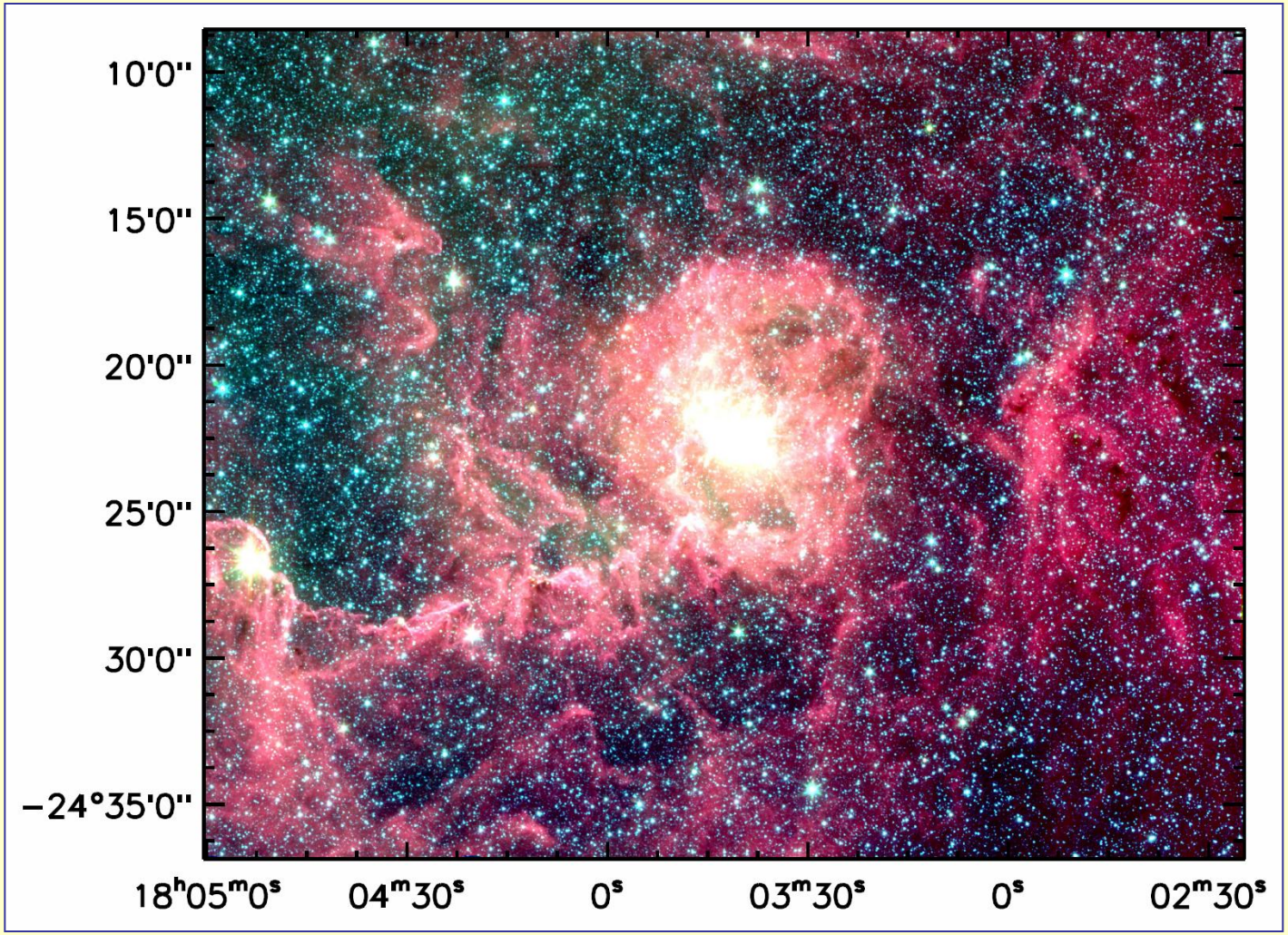

Tuthill etal 2008

Evolutionary Stages of Protostars

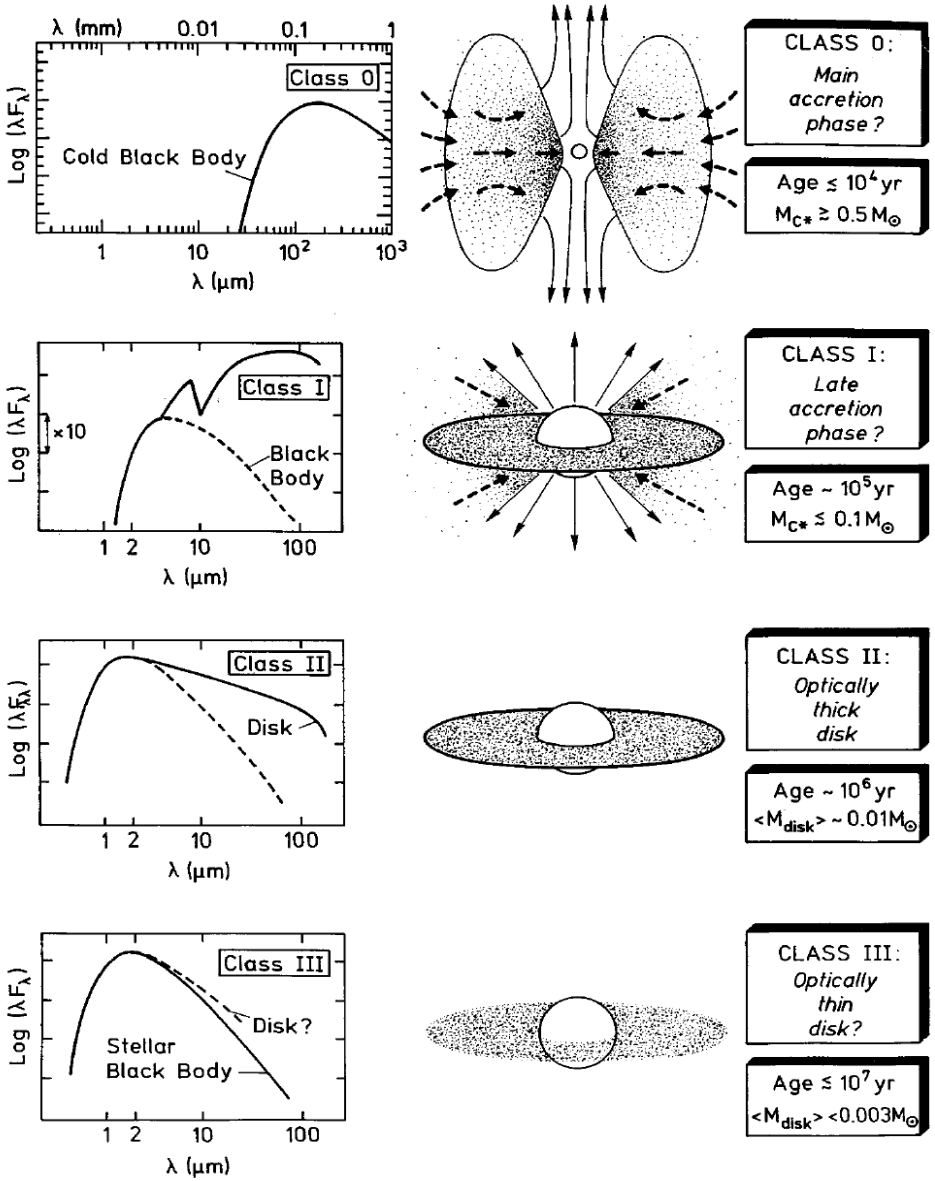

Figure 11 Evolutionary sequence of the spectral energy distributions for low-mass YSOs as proposed by André (1994). The four classes 0, I, II, and III correspond to successive stages of evolution.

Bachiller 1996

Origin of Bipolar Flows

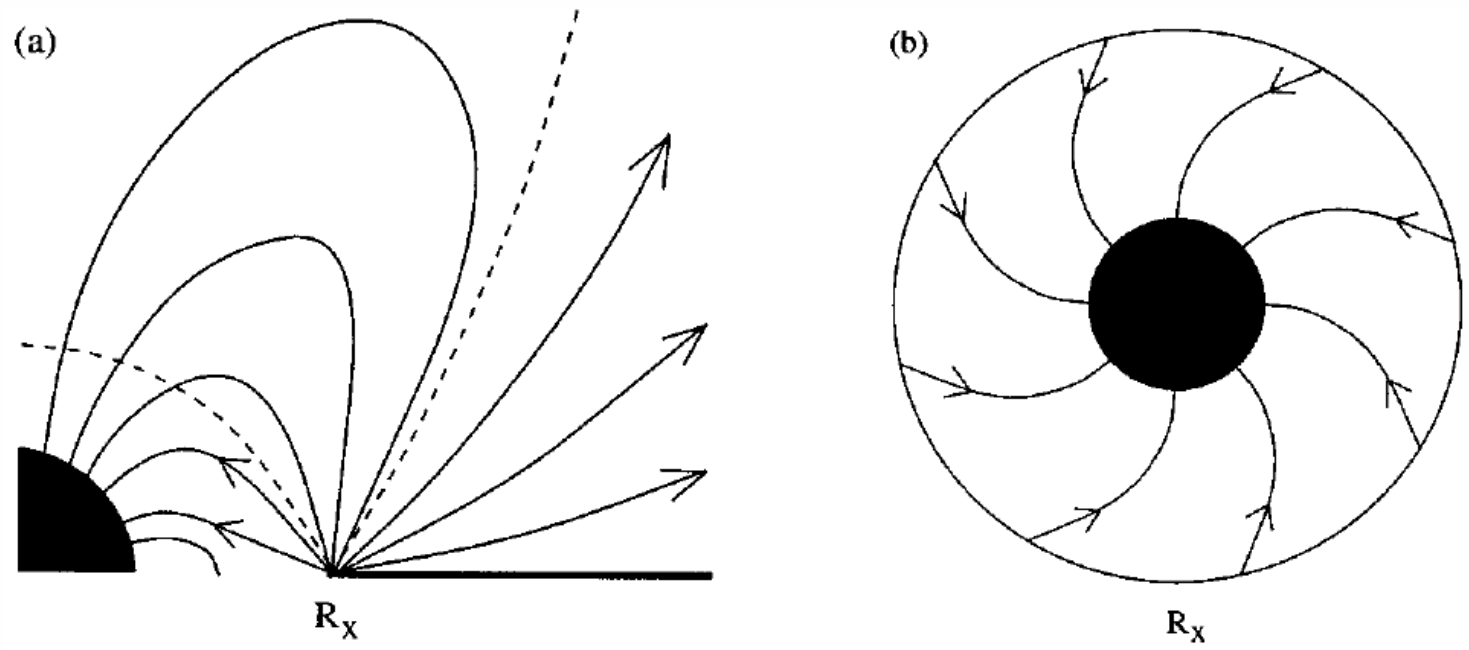

Figure 13 Schematic views of the (*a*) meridional plane and (*b*) equatorial plane of the configuration modeled by Shu et al (1994a,b) for the origin of bipolar outflows. The circumstellar disk is truncated at a distance R_X from the star. Both energetic outflows and funnel flows emerge from the disk truncation region. Gas accreting from the disk onto the star in a funnel flow drags the stellar field into a trailing spiral pattern. (From Najita 1995.)

Taken from Whittet 2003

HH Flows in Optical Lines

Figure 2 The HH 1 bow shock and jet seen with the Hubble Space Telescope. (*Red*) [SII] emission; (*blue*) Hα.

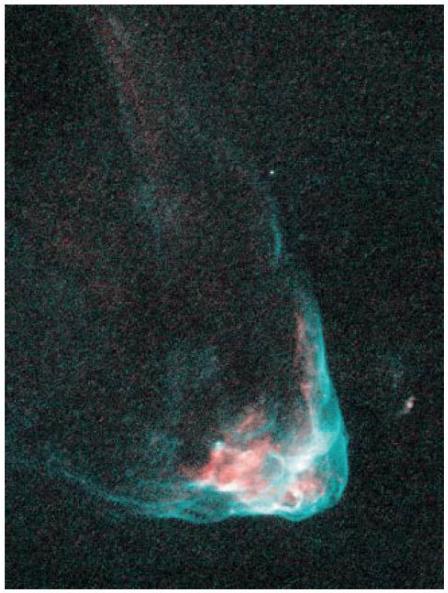

Figure 4 The HH 34 bow shock and Mach disk as seen with the Hubble Space Telescope. The high-excitation bow shock dominates in Hα (*green*) and the low-excitation Mach disk is prominent in [SII] (*red*).

Reipurth & Bally 2001

CO Lines

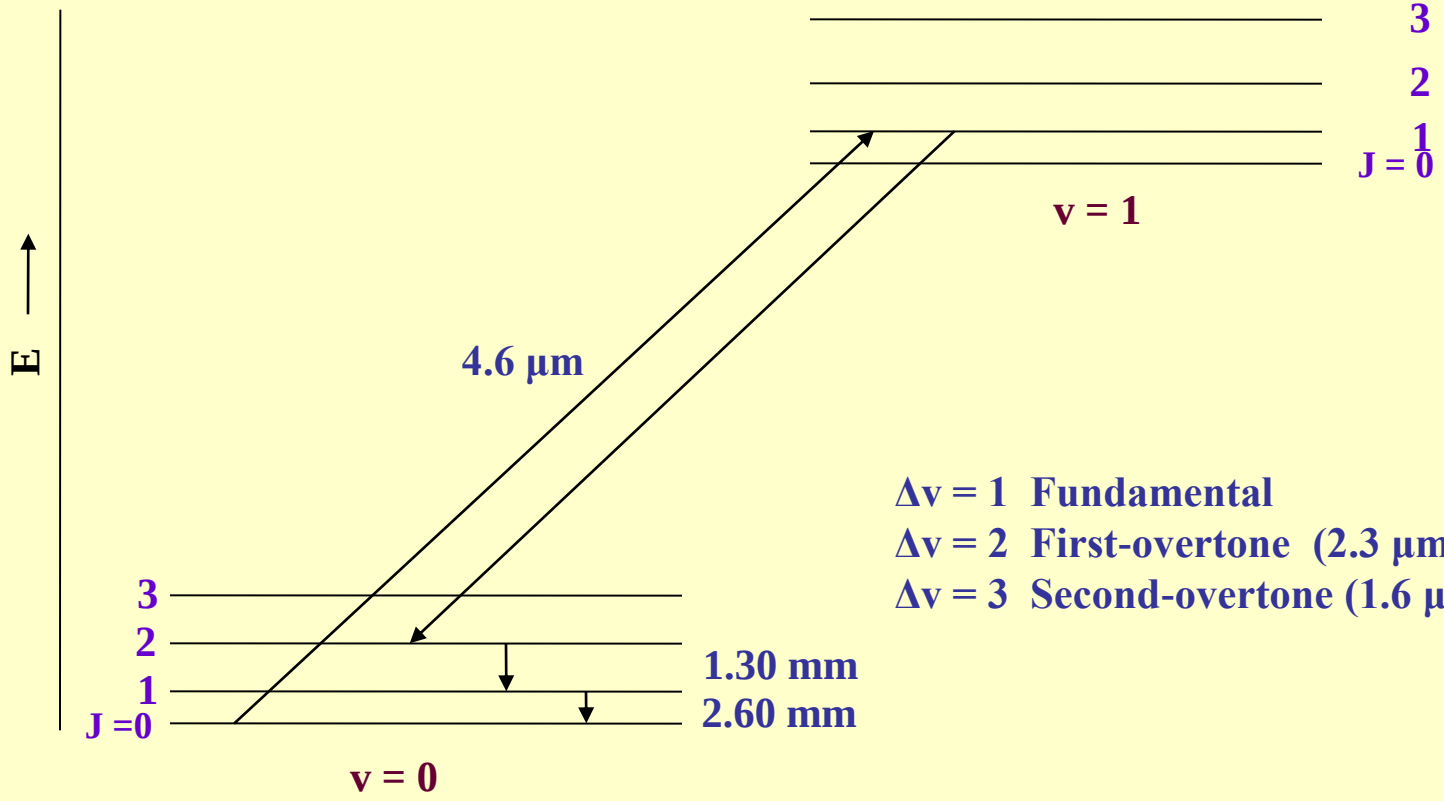

Δv = 1 Fundamental
Δv = 2 First-overtone (2.3 µm)
Δv = 3 Second-overtone (1.6 µm)

CO is formed in gas phase reactions through ion-molecule reactions

Electronic Transitions of Molecular Hydrogen

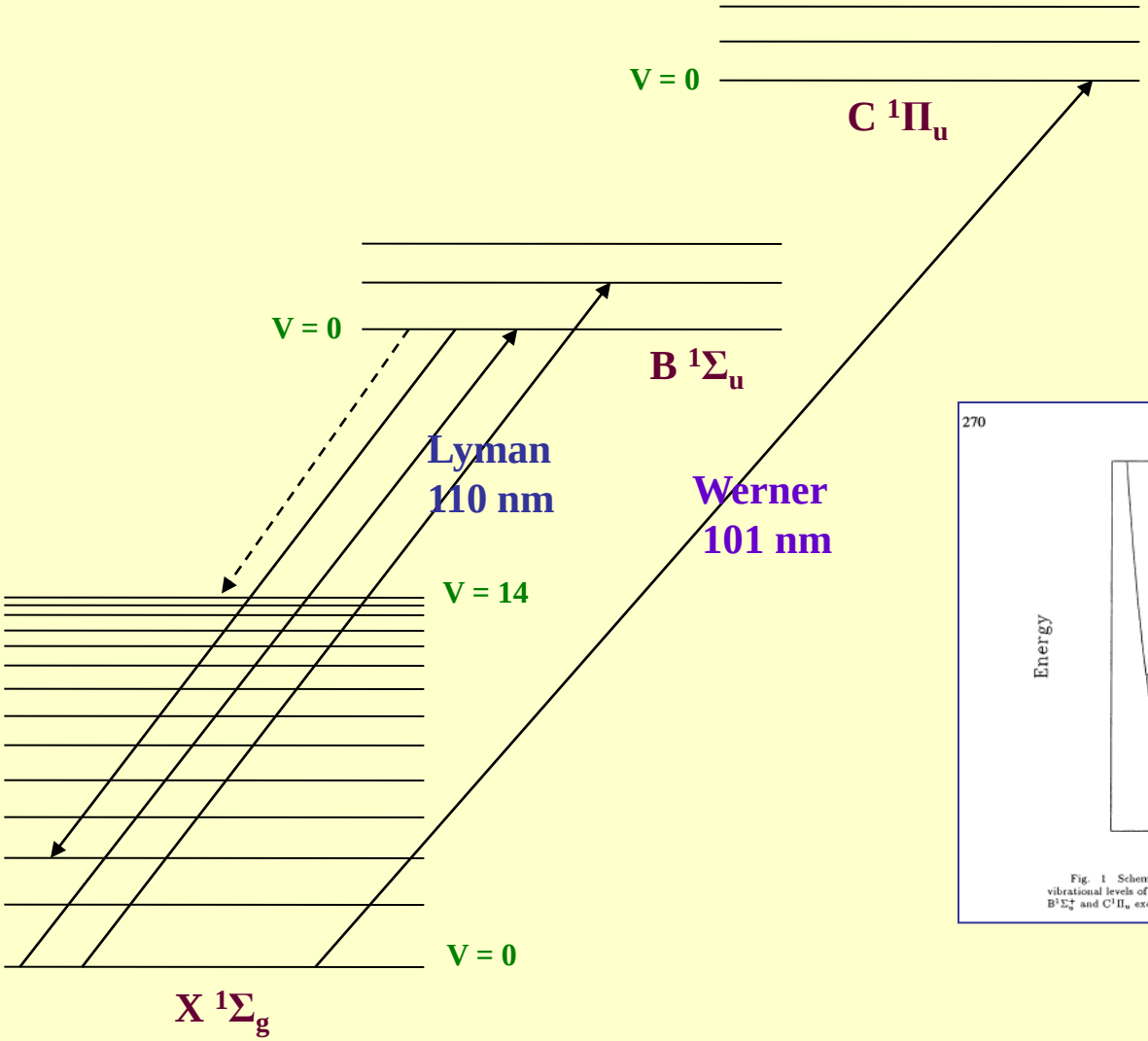

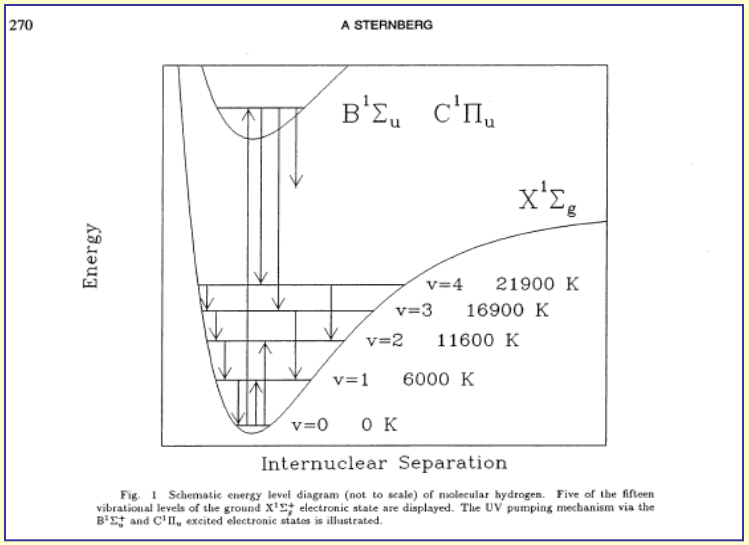

Fig. 1. Schematic energy level diagram (not to scale) of molecular hydrogen. Five of the fifteen vibrational levels of the ground $X^1\Sigma_g^+$ electronic state are displayed. The UV pumping mechanism via the $B^1\Sigma_u^+$ and $C^1\Pi_u$ excited electronic states is illustrated.

Sternberg 1989

Line Ratios as Probes

Line intensity ratio of S(1) 1-0 / S(1) 2-1 is used to probe the mechanism
2 for fluorescence and 10 for shock heating

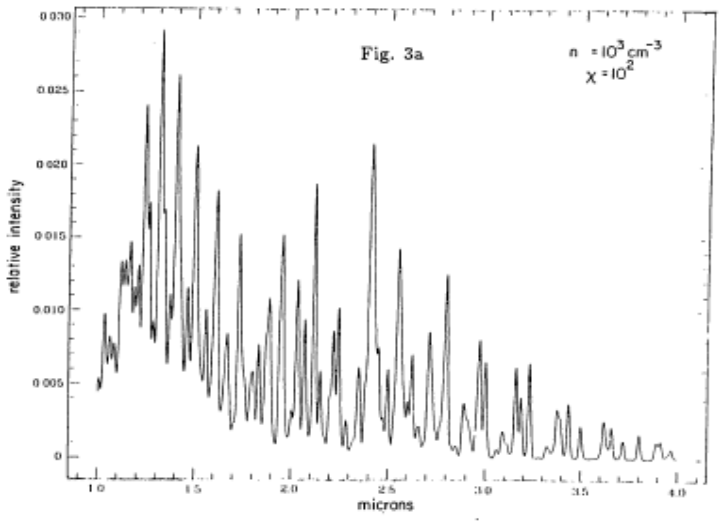

Table 1a: Radiative Fluorescent Emission Line Intensities.

μm	$100I/I_{tot}$	line	μm	$100I/I_{tot}$	line
1.16	0.67	2,0 S(1)	2.12	1.59	1,0 S(1)
1.23	0.85	3,1 S(1)	2.22	0.76	1,0 S(0)
1.31	0.79	4,2 S(1)	2.25	0.89	2,1 S(1)
1.31	0.79	3,1 Q(1)	2.41	1.36	1,0 Q(1)
1.40	0.80	4,2 Q(1)	2.41	0.84	1,0 Q(2)
1.49	0.71	5,3 Q(1)	2.42	1.12	1,0 Q(3)
1.51	0.68	4,2 O(3)	2.55	0.86	2,1 Q(1)
1.83	0.68	1,0 S(5)	2.57	0.65	2,1 Q(3)
1.96	1.26	1,0 S(3)	2.80	1.15	1,0 O(3)
2.03	0.97	1,0 S(2)	2.97	0.74	2,1 O(3)

The fractional intensities of the 20 strongest lines of the H_2 emission spectrum in the 1 to 4 micron band produced in a photodissociation region with $n = 10^3$ cm^{-3} and $\chi = 10^2$, relative to the total intensity $I_{tot} = 4.90 \times 10^{-5}$ ergs s^{-1} cm^{-2} sr^{-1} (Ref. 102). This spectrum is displayed graphically in Fig. 3a.

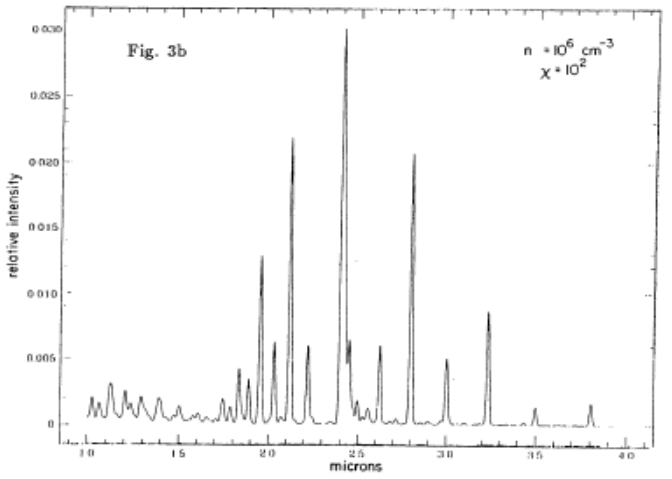

Sternberg 1989

Table 1b: LTE Emission Line Intensities.

μm	$100I/I_{tot}$	line	μm	$100I/I_{tot}$	line
1.75	0.16	1,0 S(7)	2.44	0.34	1,0 Q(4)
1.83	0.40	1,0 S(5)	2.45	0.62	1,0 Q(5)
1.89	0.26	1,0 S(4)	2.47	0.12	1,0 Q(6)
1.96	1.27	1,0 S(3)	2.50	0.18	1,0 Q(7)
2.03	0.61	1,0 S(2)	2.63	0.59	1,0 O(2)
2.12	2.17	1,0 S(1)	2.80	2.07	1,0 O(3)
2.22	0.59	1,0 S(0)	3.00	0.50	1,0 O(4)
2.41	2.44	1,0 Q(1)	3.23	0.86	1,0 O(5)
2.41	0.65	1,0 Q(2)	3.50	0.14	1,0 O(6)
2.42	1.53	1,0 Q(3)	3.81	0.17	1,0 O(7)

The fractional intensities of the 20 strongest lines of the H_2 emission spectrum in the 1 to 4 micron band produced in a photodissociation region with $n = 10^6$ cm^{-3} and $\chi = 10^2$, relative to the total intensity $I_{tot} = 5.38 \times 10^{-5}$ ergs s^{-1} cm^{-2} sr^{-1} (Ref 102). This spectrum is displayed graphically in Fig. 3b.

Require other line ratios – particularly the upper vibrational levels

Shocked Regions

Radiative / J Shocks

Fast (~ 100 km/s)
Dissociate Molecules;
Re-formation in the wakes at T = 500 K

Continuous / C Shocks

Slow (~ 30 km/s) (non-dissociative)
Thermal Spectrum

Degree of Excitation vs Shock Velocity

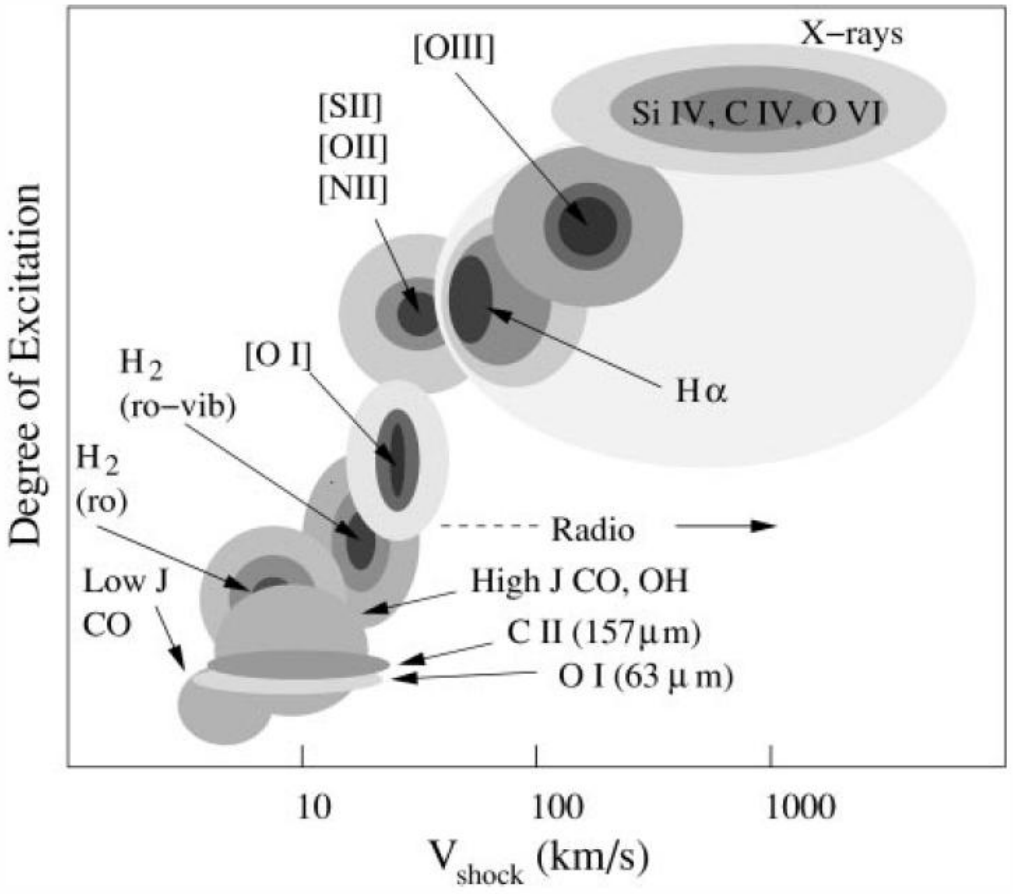

Reipurth & Bally 2001

CO Outflows from PMS Stars

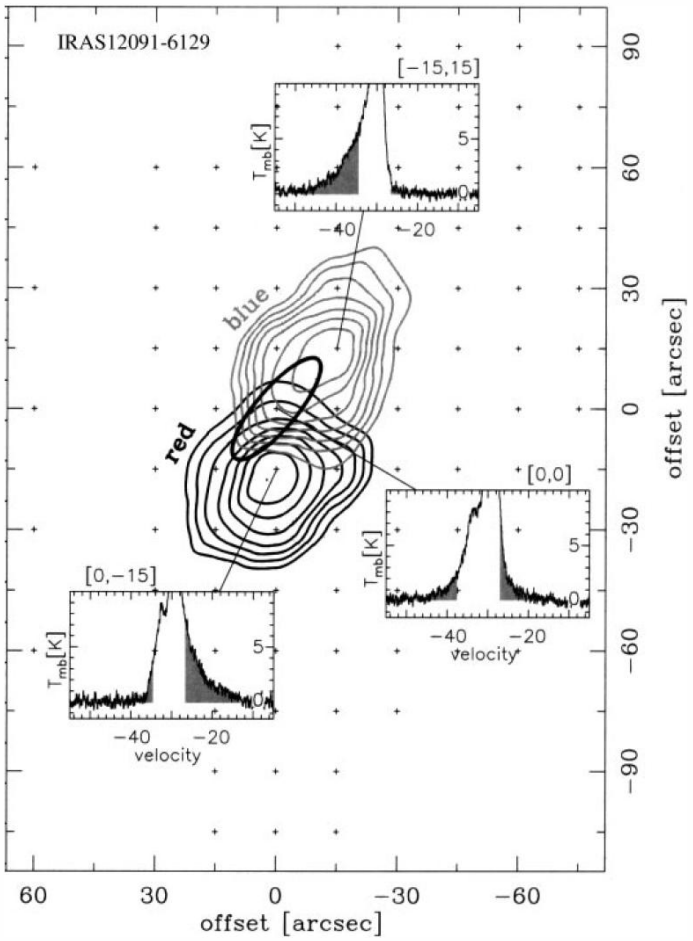

Figure 6 The CO outflow presumably driven by the FIR source IRAS12091-6129 from Henning et al. (2000). This figure illustrates three general properties of outflows driven by massive protostars: low outflow speeds, poor collimation, and large masses. The arbitrary cutoff velocities (shaded regions in the spectra) for the outflow also illustrate why outflow masses are uncertain and different authors disagree on the estimated masses.

Churchwell 2003

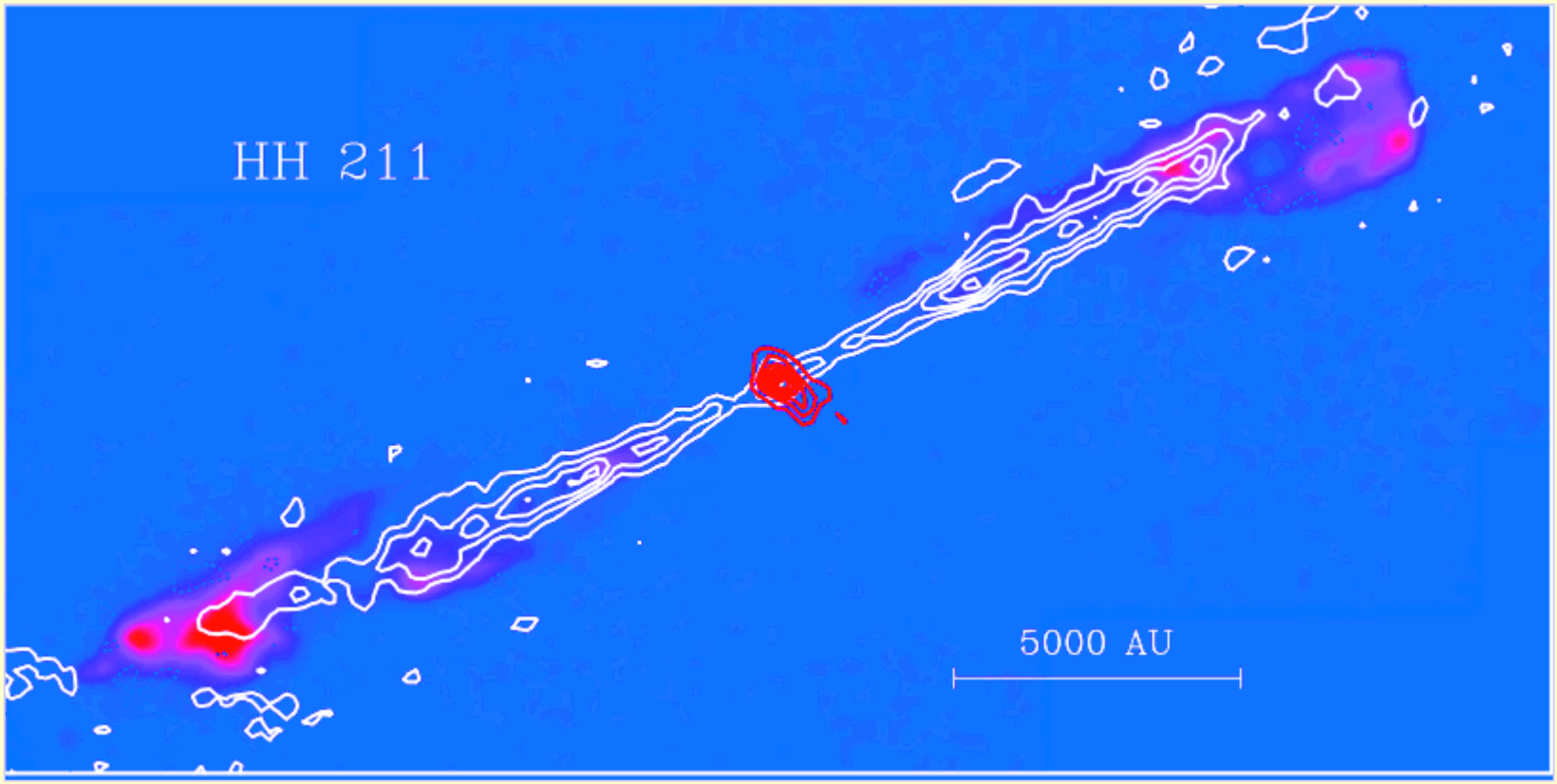

Interferometer map of the molecular jet in the HH211 outflow;

the CO emission (white lines) is overlaid on a false color image of excited molecular hydrogen.

The red lines delineate a flattened dust concentration around the protostar.

From IRAM website

Massive Young Star
Embedded in a Dense Molecular Cloud

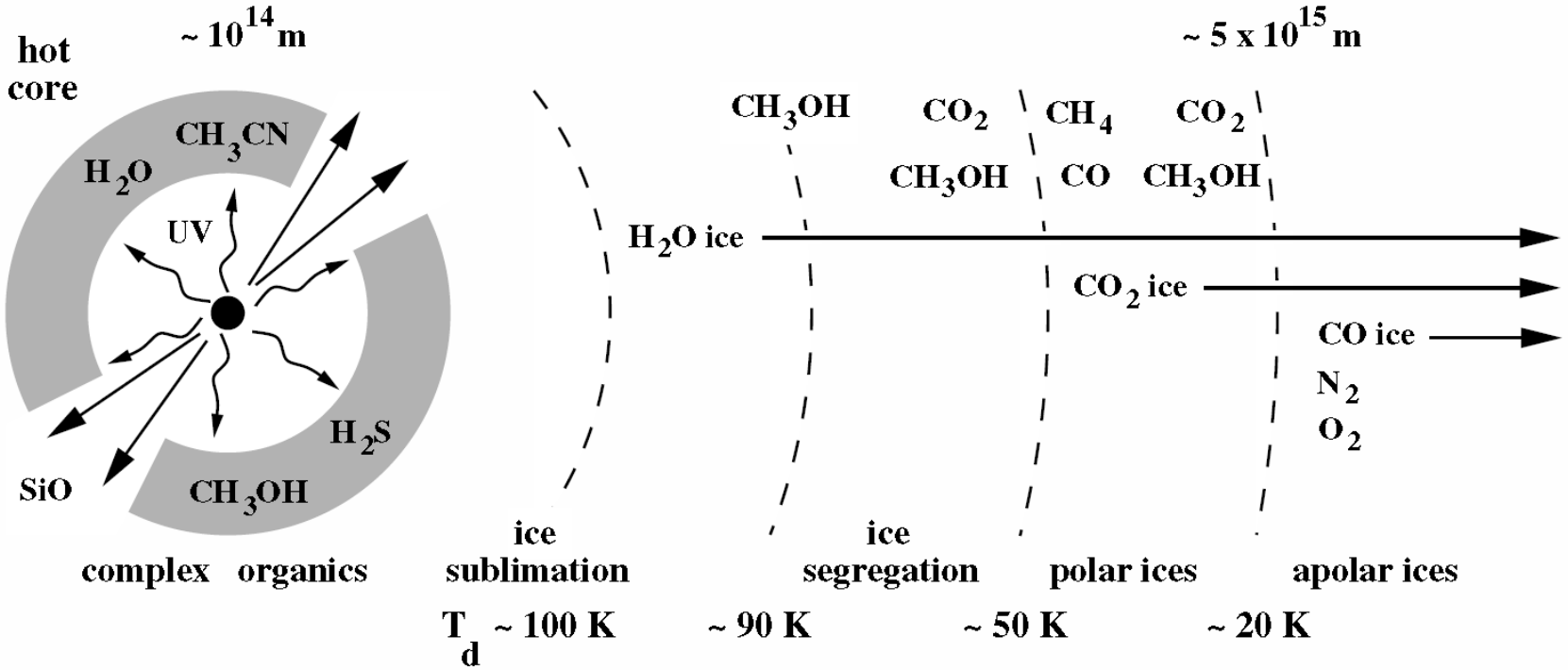

Van Dishoeck & Blake 1998

Infrared Solid State (ice) Features from a Protostar

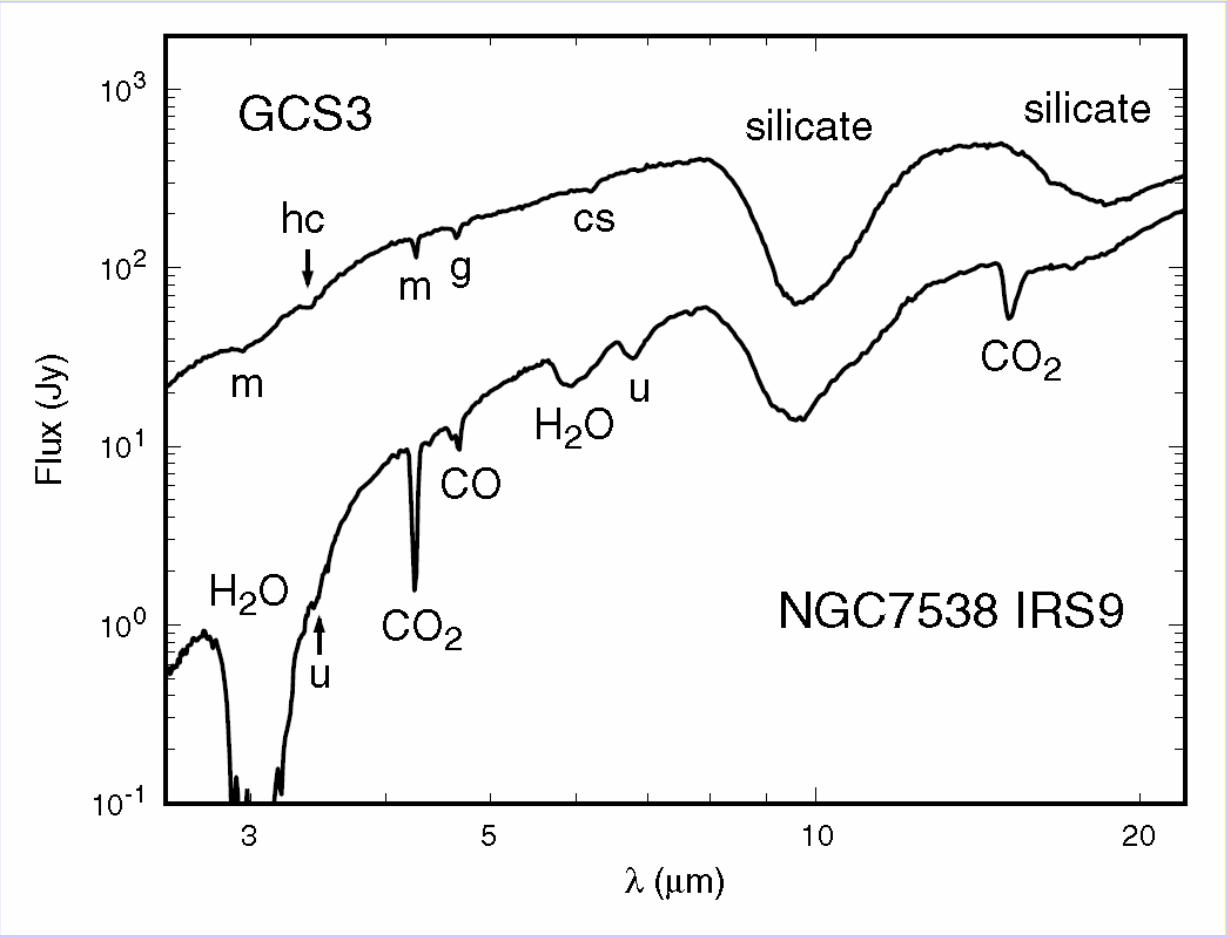

Whittet 2003

Spatial Structure in the Molecular Hydrogen Jets from the Low Mass Young Stellar Object RNO 91 having a debris disk with ice features

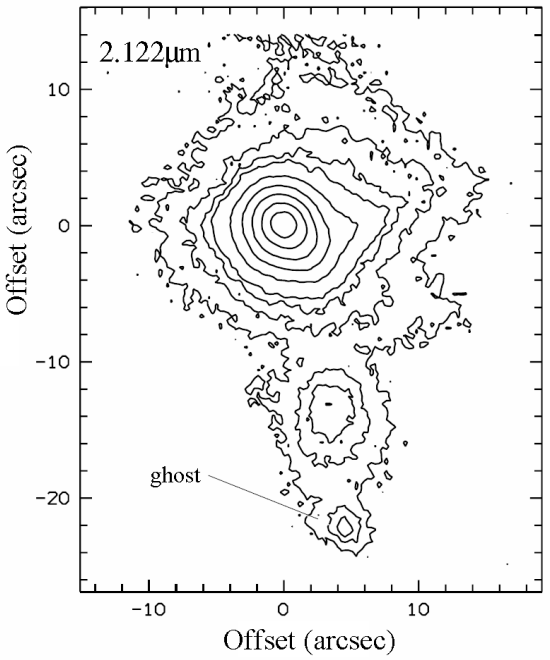

Fig. 3. Contour plot of RNO91 taken through narrowband filter, illustrating an east-west disk associated with the source, as well as nebulous emission to the south. The contours measure 5, 10, 15, 20, 40, 80, 160, 320 and 640× the standard deviation to the mean background level in the image.

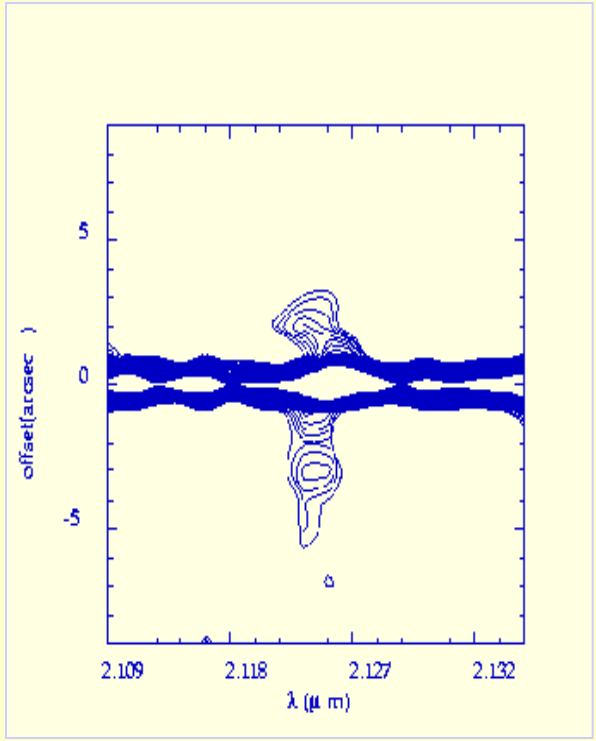

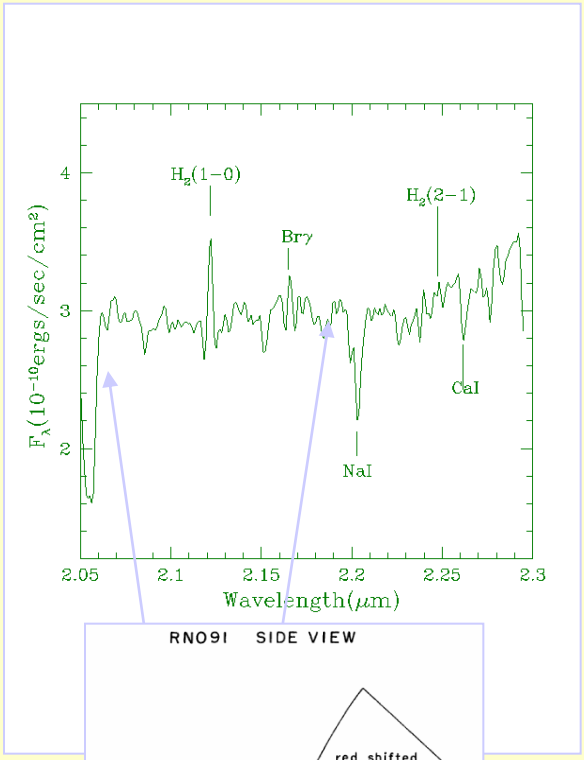

Shock excitation at low densities

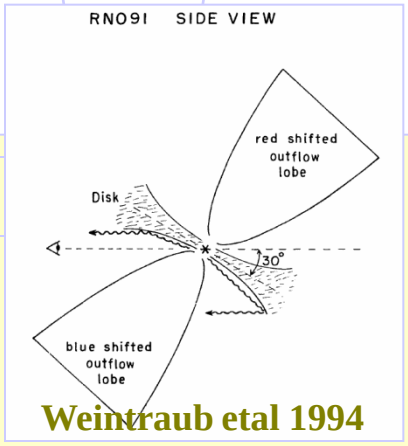

Weintraub etal 1994

Nandakumar, Anandarao & Davis 1999

High Mass Star Forming Region IRAS 06061+2151

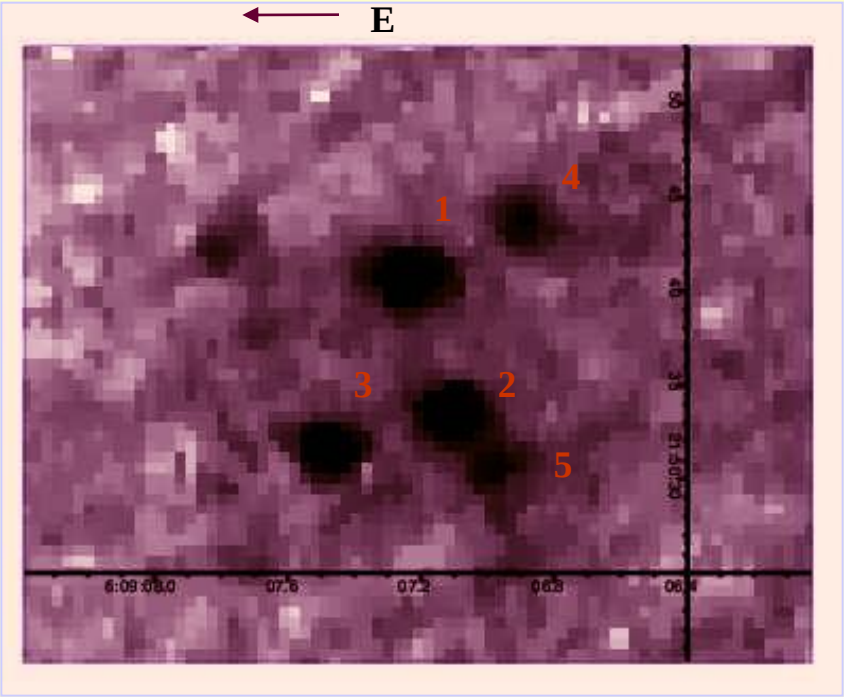

K′ Band image of IRAS 06061+2151 observed from Mt. Abu. The numbers represent sources of IRAS 06061+2151.

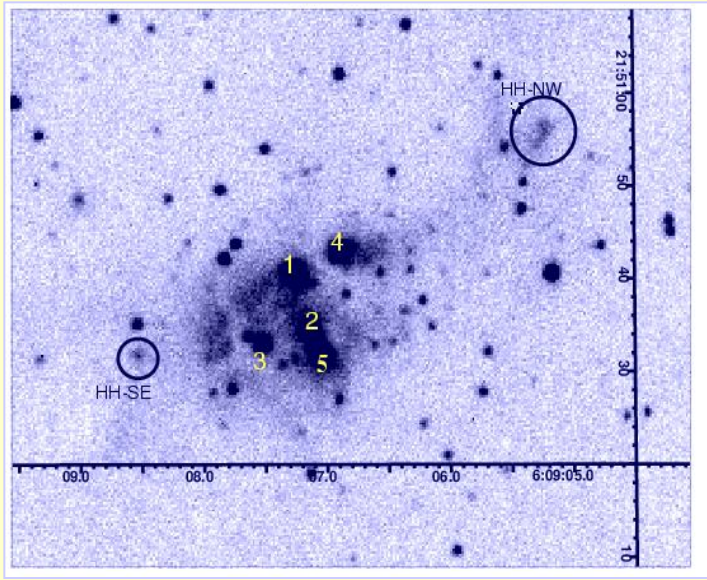

H_2 (2.12 μm) line image

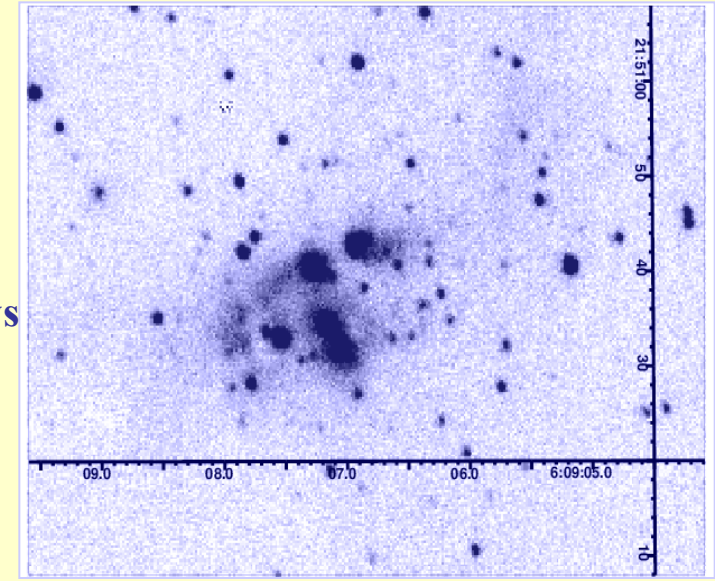

Br γ (2.16 μm) line image

- Presence of knots in H_2 and absence in Brγ shows a mild shock (~ 30 km/s) by the outflow from the massive star (star 4 of B0 type)
- It is also indicative of an accretion disk
- Suggestive of formation by accretion
- Jet extent 0.5 pc

Anandarao et al 2004

TNG Narrow-band Images

High Mass Star Forming Region IRAS 06061+2151

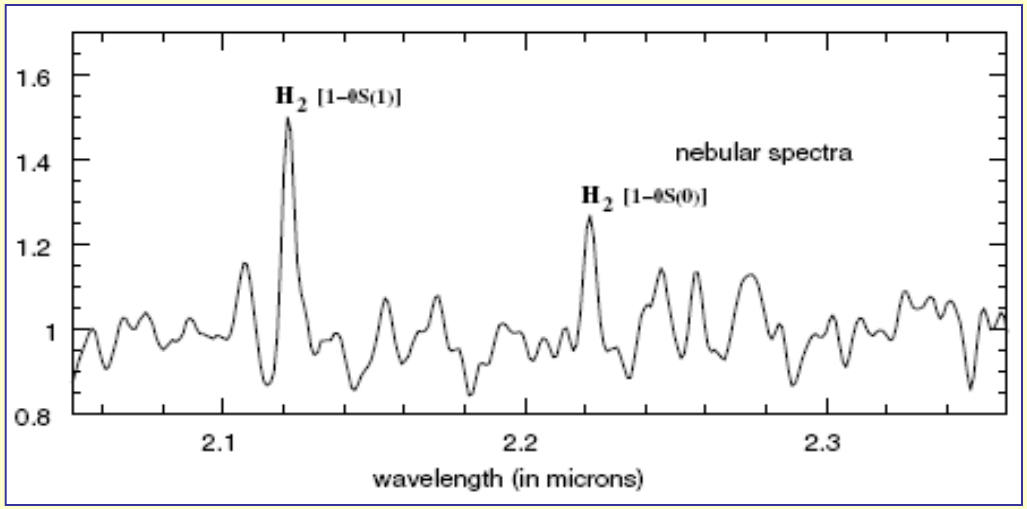

Shock-excited Molecular Hydrogen

Observed Ratios: **1-0 S(1)/ 2-1 S(1) > 10**
1-0 S(1)/1-0 S(0) ~ 2

LTE at T = 1000 K: **1-0 S(1)/ 2-1 S(1) > 10**
1-0 S(1)/1-0 S(0) ~ 3

Anandarao et al 2004

Polycyclic Aromatic Hydrocarbons

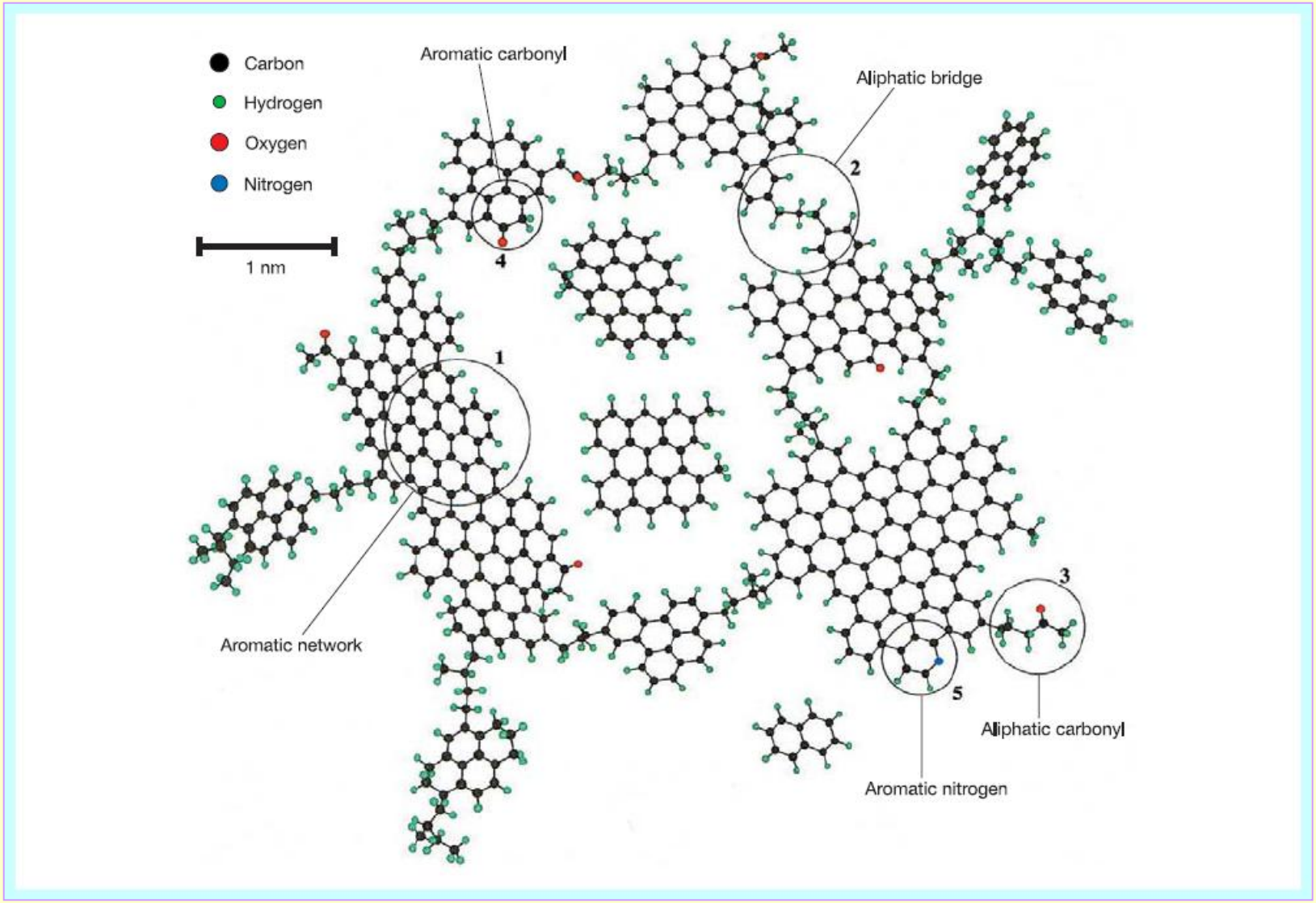

Kwok 2004

Energy Levels for a Neutral PAH

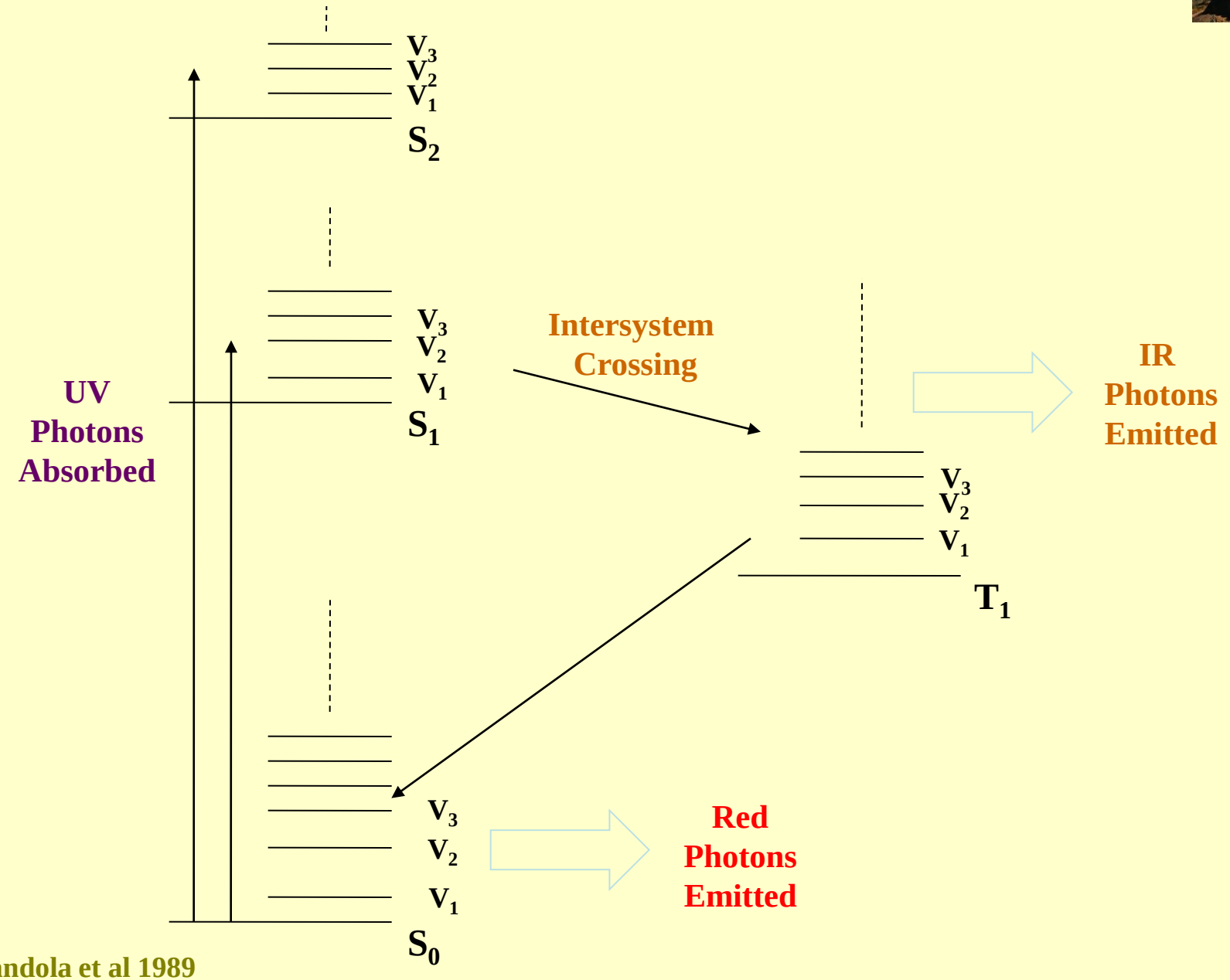

Allamandola et al 1989

Energy Levels for a Neutral PAH

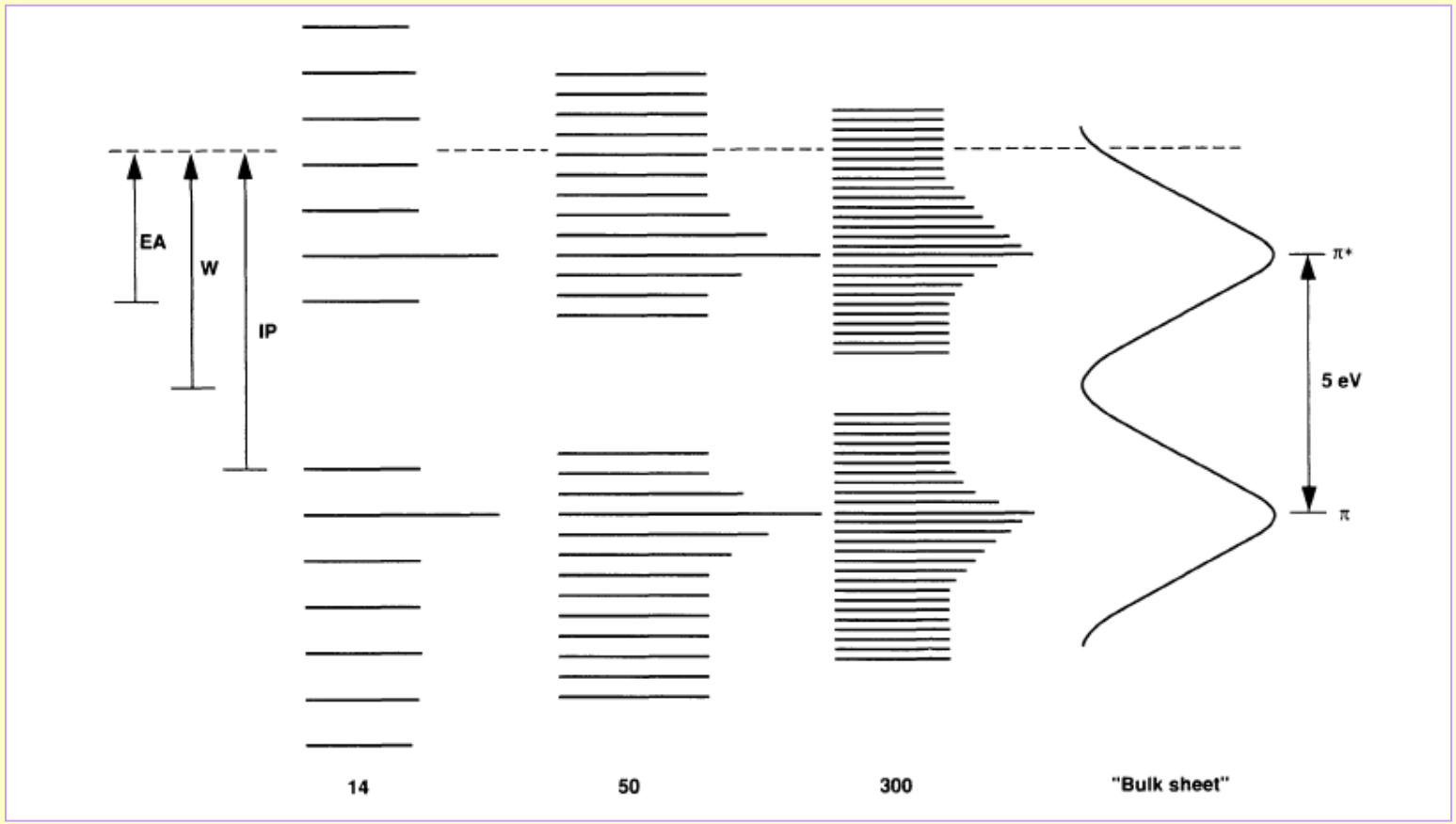

Bakes and Tielens 1994

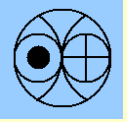

Spectral Features of Circumstellar Dust

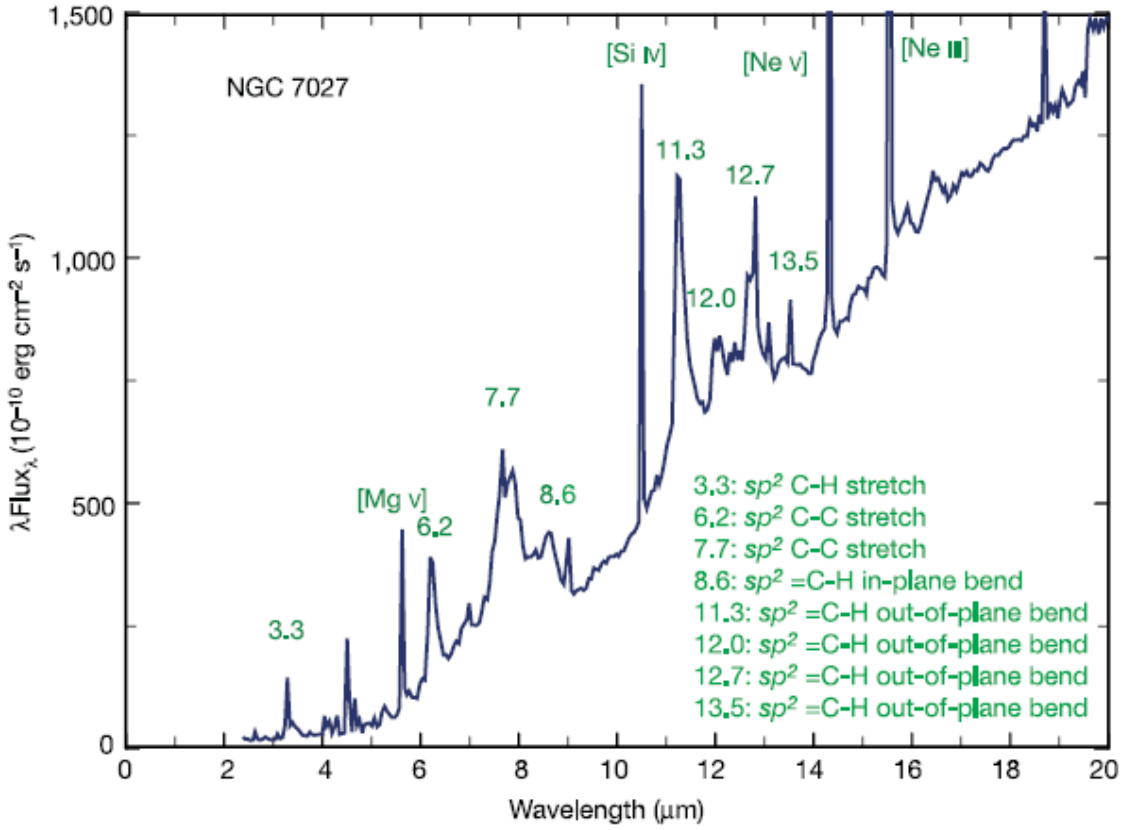

Kwok 2004

Infrared Spectra of Massive YSOs

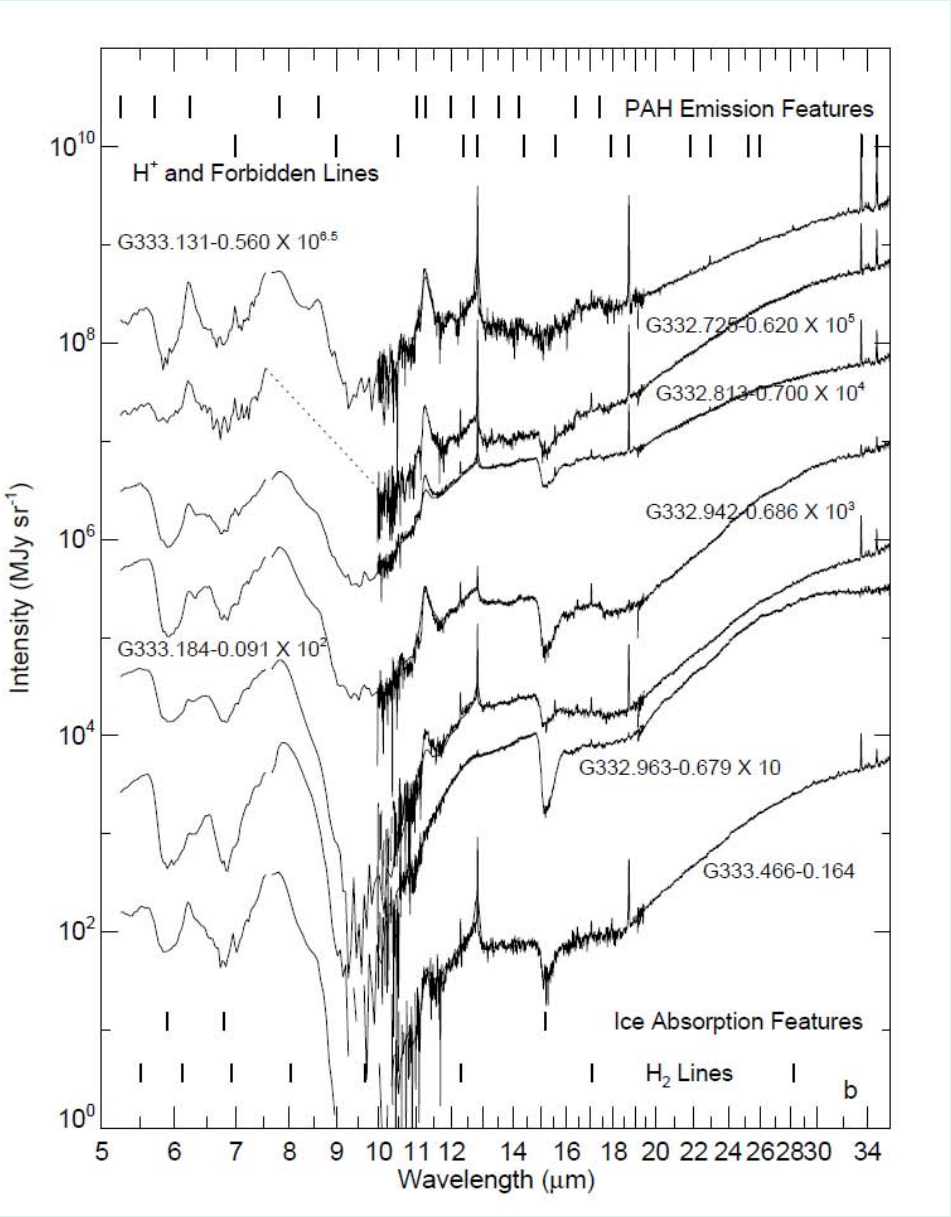

SPITZER Infrared Spectrograph on Star Forming Complex G333.2-0.4

Simpson etal 2011

M8 – Expansion of HII region

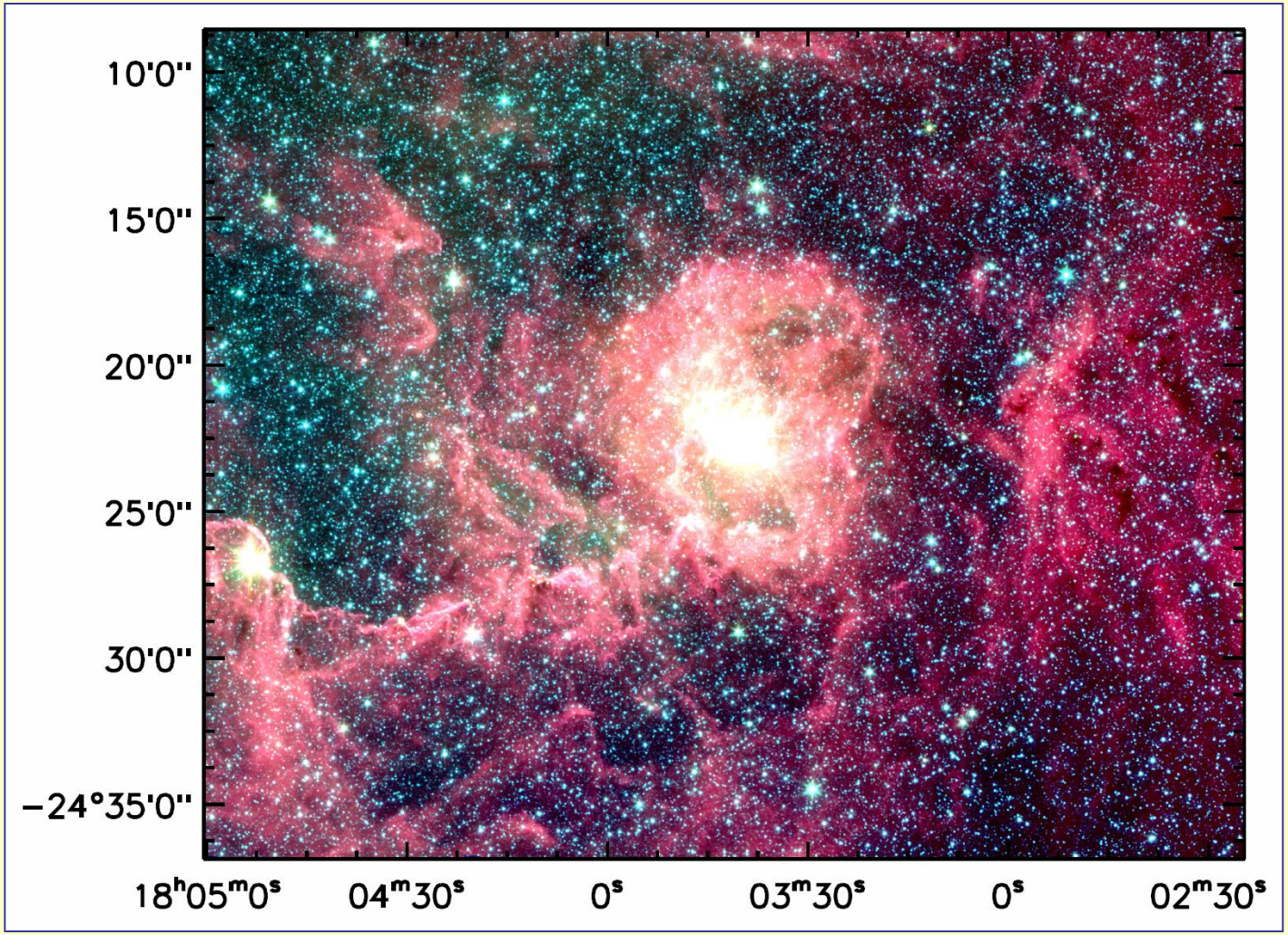

Tuthill etal 2008

Photo-Dissociation Regions

(Photon-Dominated Regions)

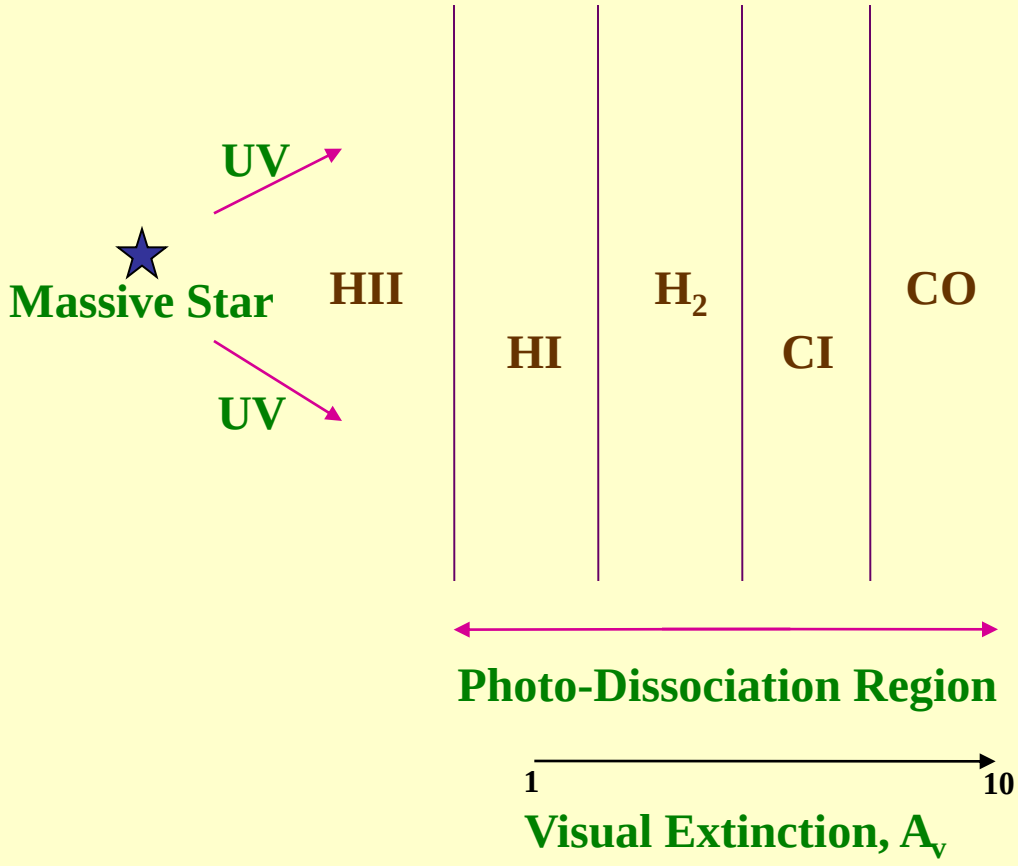

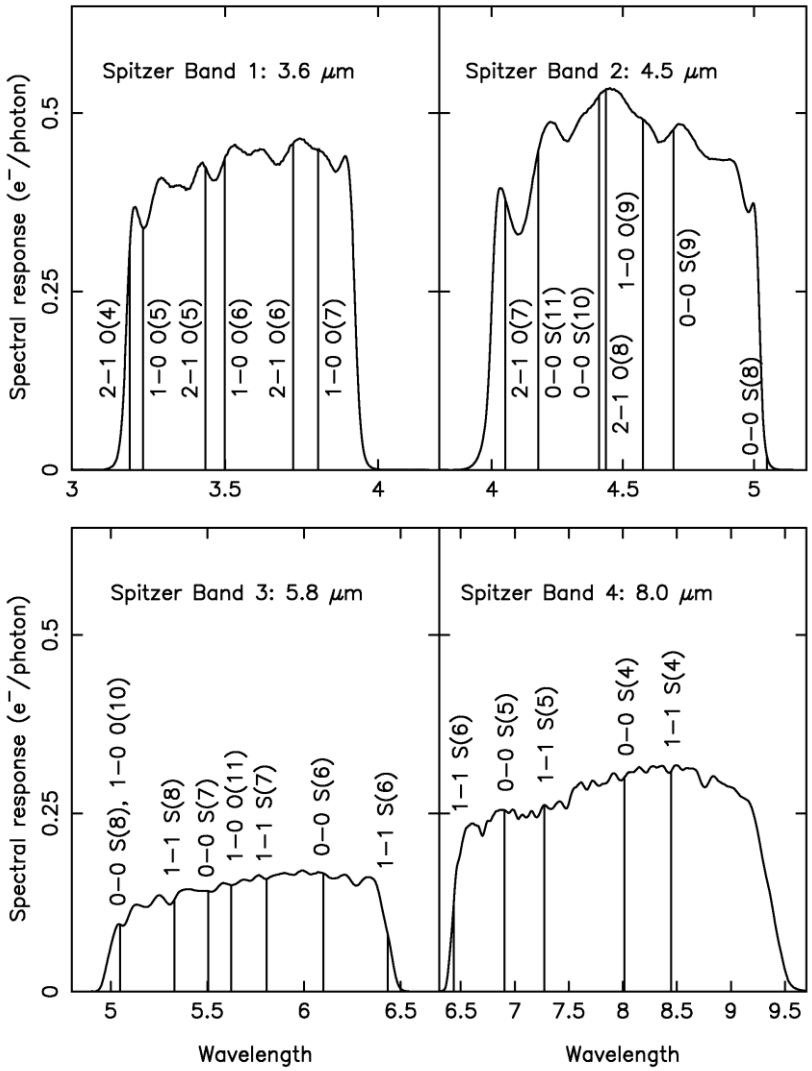

Figure 1. The spectral response functions for the four *Spitzer* IRAC bands and the spectral locations of the many contributing molecular hydrogen lines. Fluxes are derived in the simulations for each pixel and for each line and then multiplied by the spectral response before summing up to yield the band flux.

SPITZER

4 Band Photometry

Ratio Images

Identification of Atomic/Molecular/Dust Lines/Features

PAH features are present only in Bands 1, 3 and 4; Hence band 2 can be used a control

λ_{obs} (μm)	λ_{lab} (μm)	Assignments
3.29	3.29	C–H stretch
6.2	6.2	C–C stretch
7.7	7.6–8.0	C–C stretch
8.6	8.6–8.8	C–H in-plane bend
11.3, 12.7	11.2–12.7	C–H out-of-plane bend

Smith & Rosen 2005;
Povich et al 2007, 2009;
Neufeld & Yuan 2008

M17 – Multi-wavelength Observations

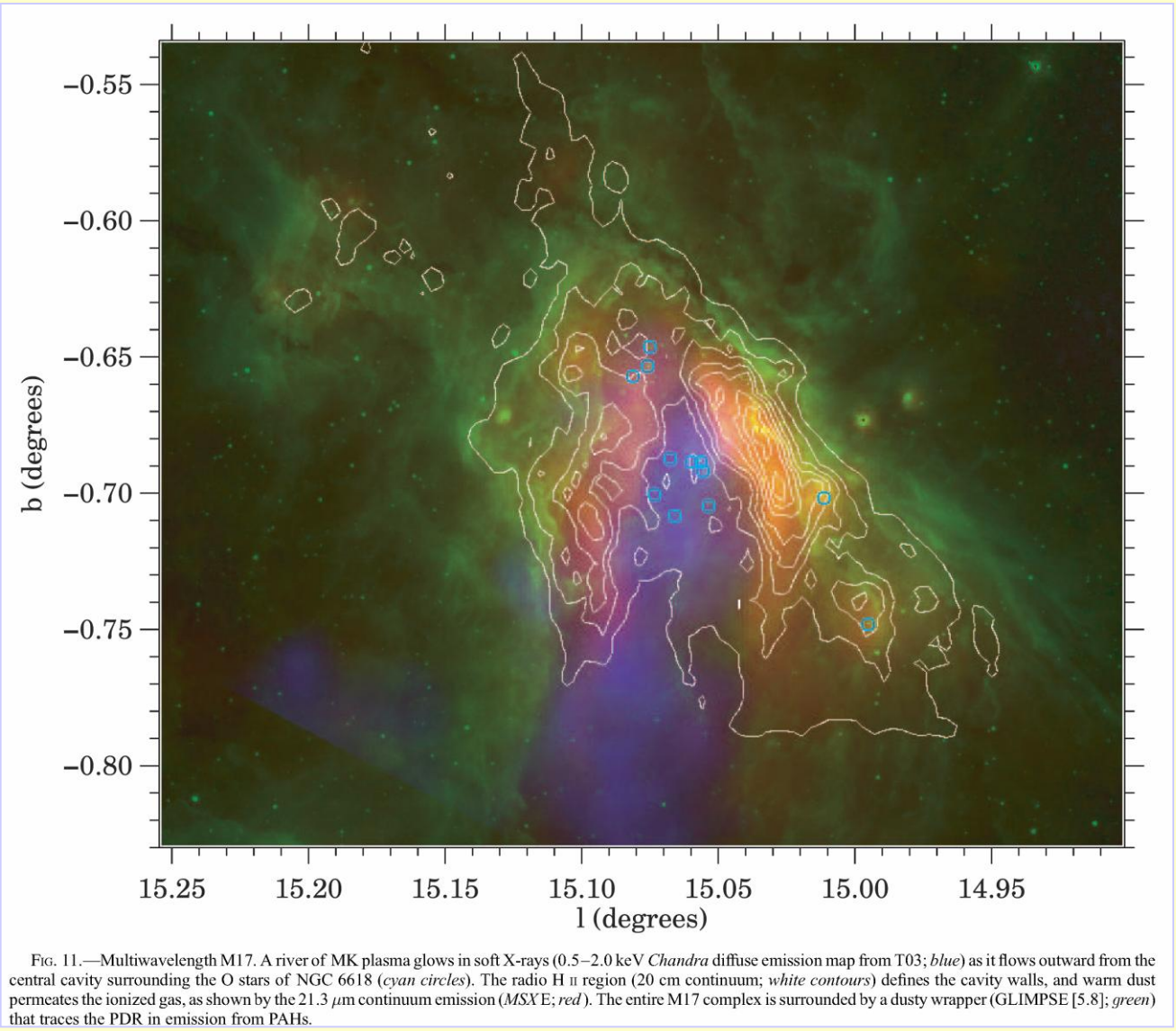

FIG. 11.—Multiwavelength M17. A river of MK plasma glows in soft X-rays (0.5–2.0 keV *Chandra* diffuse emission map from T03; *blue*) as it flows outward from the central cavity surrounding the O stars of NGC 6618 (*cyan circles*). The radio H II region (20 cm continuum; *white contours*) defines the cavity walls, and warm dust permeates the ionized gas, as shown by the 21.3 μm continuum emission (*MSX* E; *red*). The entire M17 complex is surrounded by a dusty wrapper (GLIMPSE [5.8]; *green*) that traces the PDR in emission from PAHs.

Ratio Maps:
PAH destruction by EUV photons;
Traces the PAH excitation regions of higher extinction

Povich etal 2007

AFGL 437 – Star Forming Region

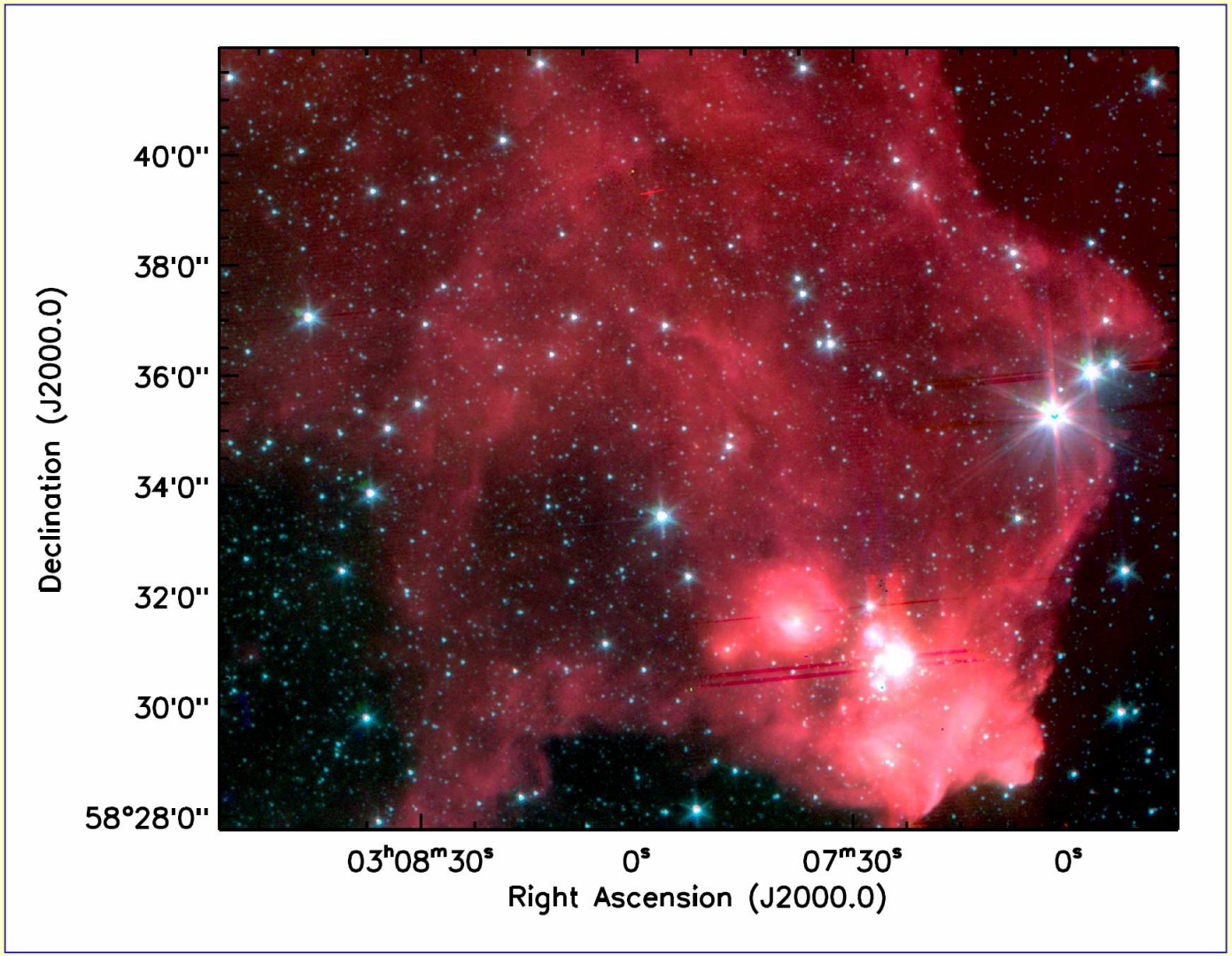

Dewanagan and Anandarao MNRAS 2010a

AFGL 437 – Ratio Maps

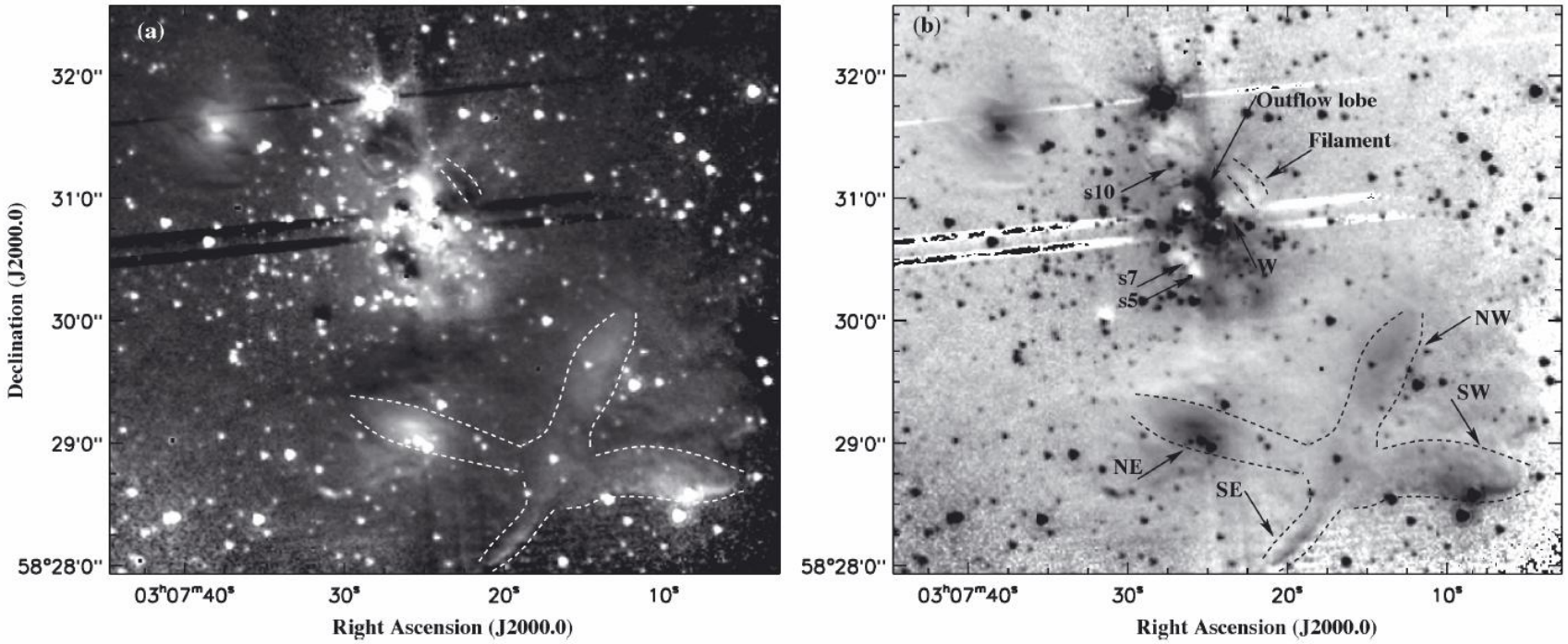

Figure 4. IRAC Ch2/Ch4 (a) and Ch4/Ch2 (b) ratio images in log scale (from mosaics made with pixel ratio of 2). The central cluster and the cross- or boxcar-like structure to its south-west can be noticed. This structure has a size of 1.7 pc in the NE–SW and 1.5 pc in NW–SE directions. The bright patches in the image on the left (a) show regions dominated by H_2 emission, while in the image on the right (b) the bright patches indicate regions that are emitting PAH bands. The prominent outflow lobe, some of the YSOs and the H_2 emission patches in the four corners of the cross-like structure are marked (by dashed curves). The near-horizontal tracks across the image are artefacts. The filament-like structure to the right of AFGL 437W is marked by dashed lines in the upper half of the figure.

Dewanagan and Anandarao MNRAS 2010a

AFGL 437 – Detection of H_2 outflow from massive YSO

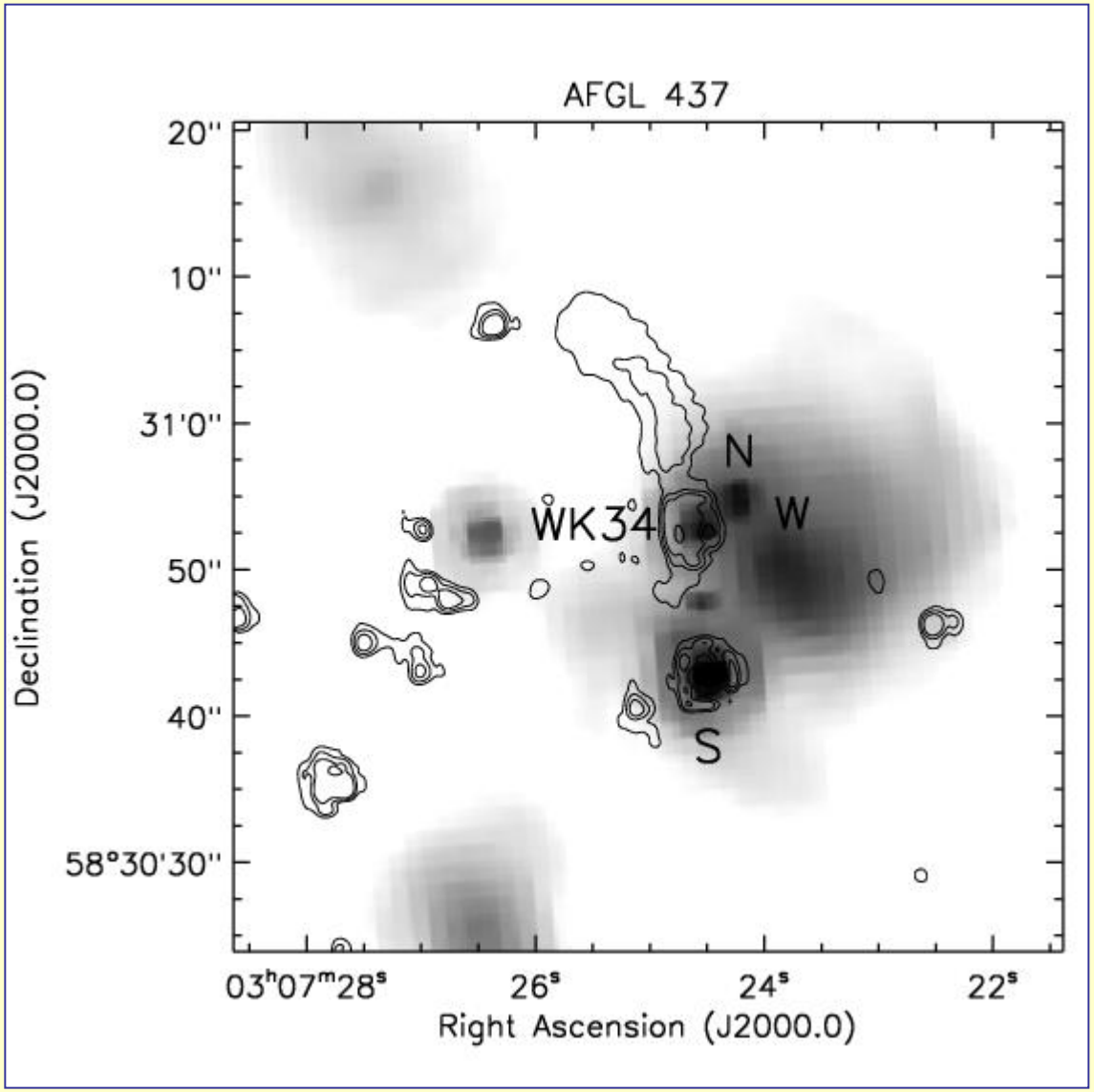

Dewanagan and Anandarao MNRAS 2010a

SED Modeling of YSOs

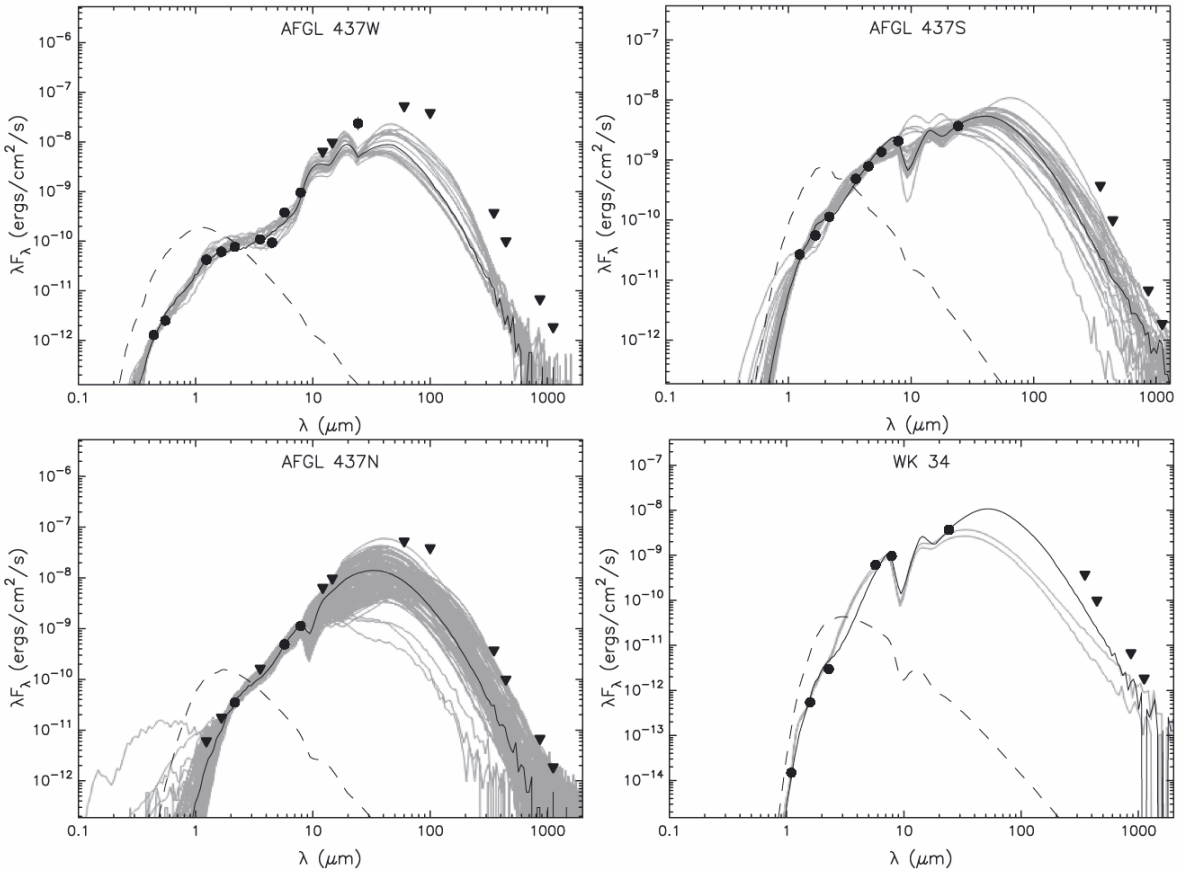

Figure 6. SEDs for four YSOs in the central cluster: AFGL 437W, S (top panels) N and WK34 (bottom panels). Filled circles are observed fluxes of good quality (with filled triangles as upper limits) taken from archives or published literature (see text for references) and the curves show the model fits. The thin black curve corresponds to the best model. The dashed curves represent photospheric contributions. The model parameters of the YSOs are listed in Table 2.

WK 34 Model Results: Age ~ 9 x 10^3 yrs; M = 7 $M_\odot$; T = 5100 K; L = 1000 $L_\odot$; A_V = 23 mag

Dewanagan and Anandarao MNRAS 2010a

M8 – Star Forming Region

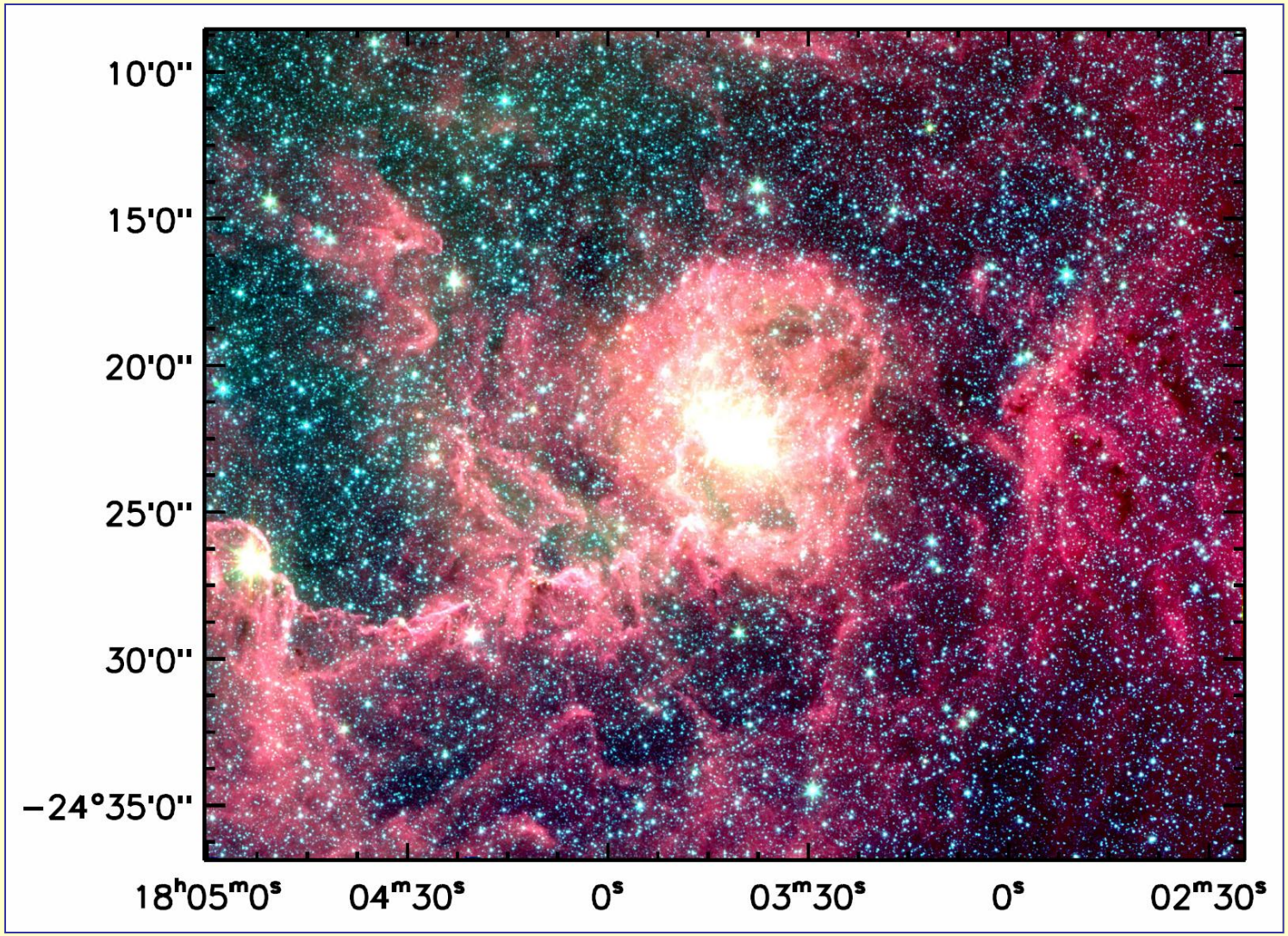

Tuthill etal 2008

Star Formation Scenario in M8

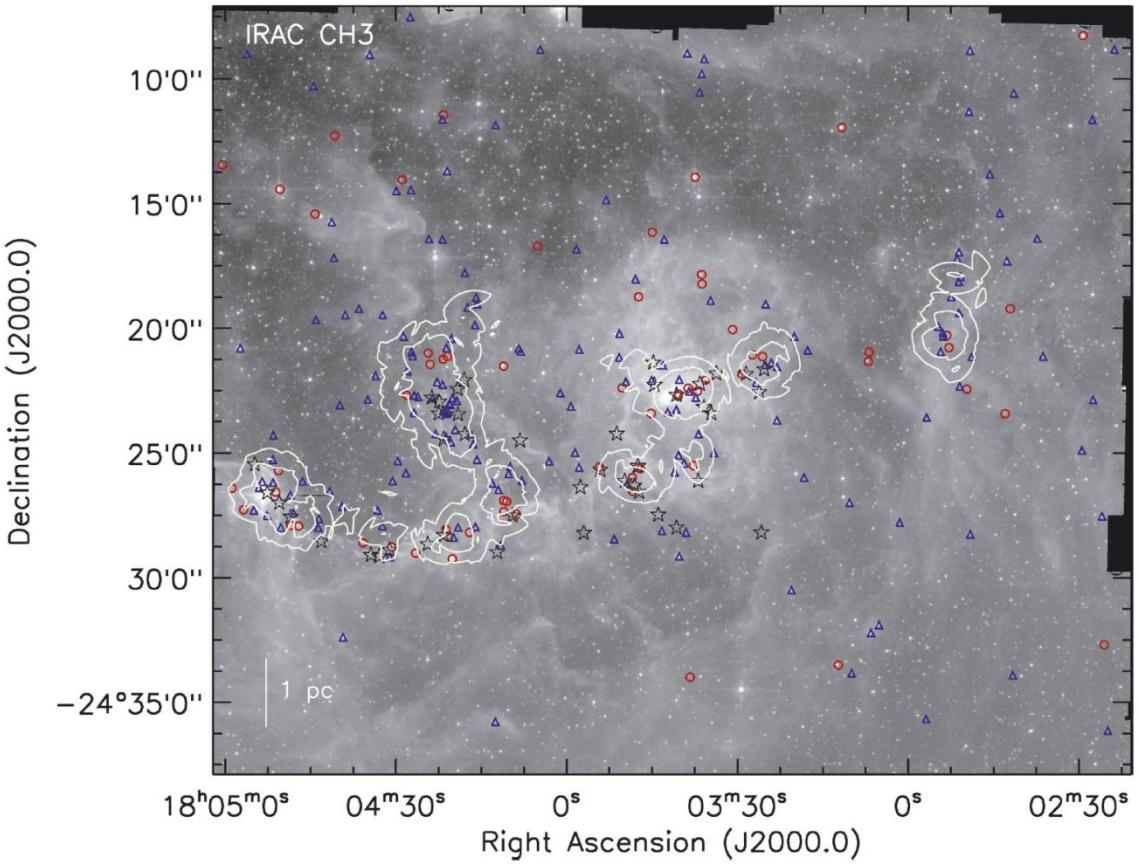

Figure 4. *Spitzer* IRAC Ch3 (5.8 μm) image of M8 (~42.5 × 30.0 arcmin^2) superposed by IRAC class 0/I and class II sources and submm gas clumps. The open circles (red) and open triangles (blue) show the IRAC class 0/I and class II sources, respectively (from Tables 1 and 2). The black star symbols represent the locations of the submm gas clumps (from table 1 of Tothill et al. 2008). The overlaid contours (white) are YSO density contours generated using a grid size of 5 arcsec; the inner contours are 10 YSOs pc^{-2} and the outer contours represent 5 YSOs pc^{-2}.

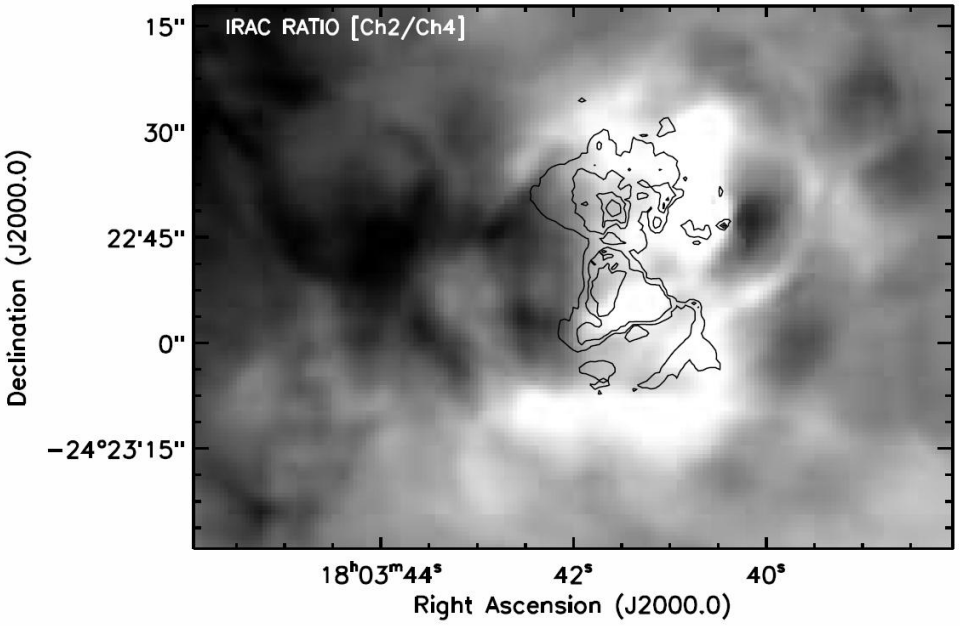

(a)

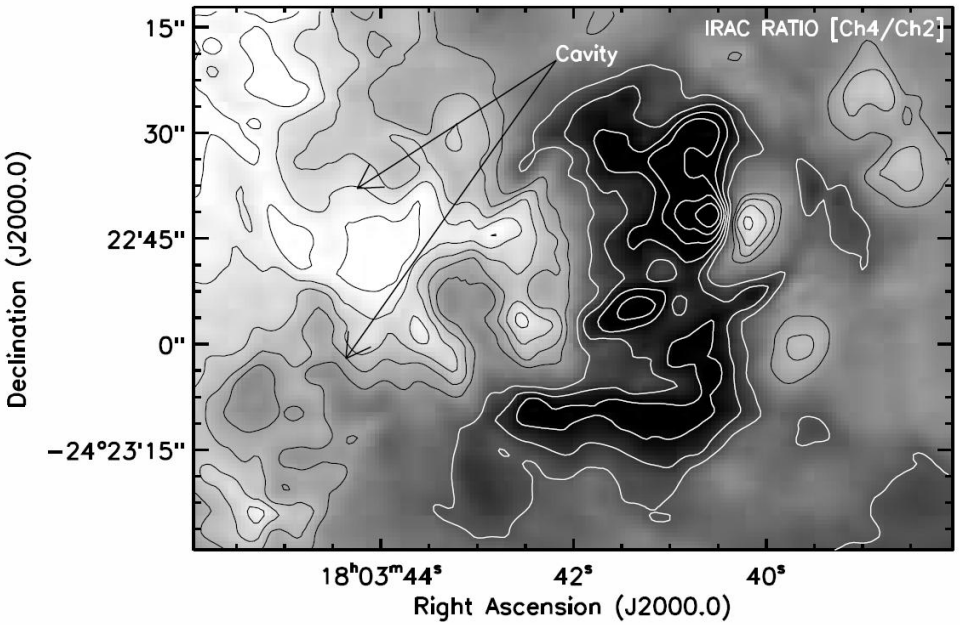

(b)

A Cavity of PAH emission

The bright 3-like figure in Ch2/Ch4 Traces probably the Br alpha line in Ch2 rather than molecular Hydrogen (as Burton's (2002) maps show no trace of it)

To the left of Hour Glass Region a PAH region is found and traces the edge of HII region (bright regions in Ch4/Ch2)

Dewanagan and Anandarao MNRAS 2010b

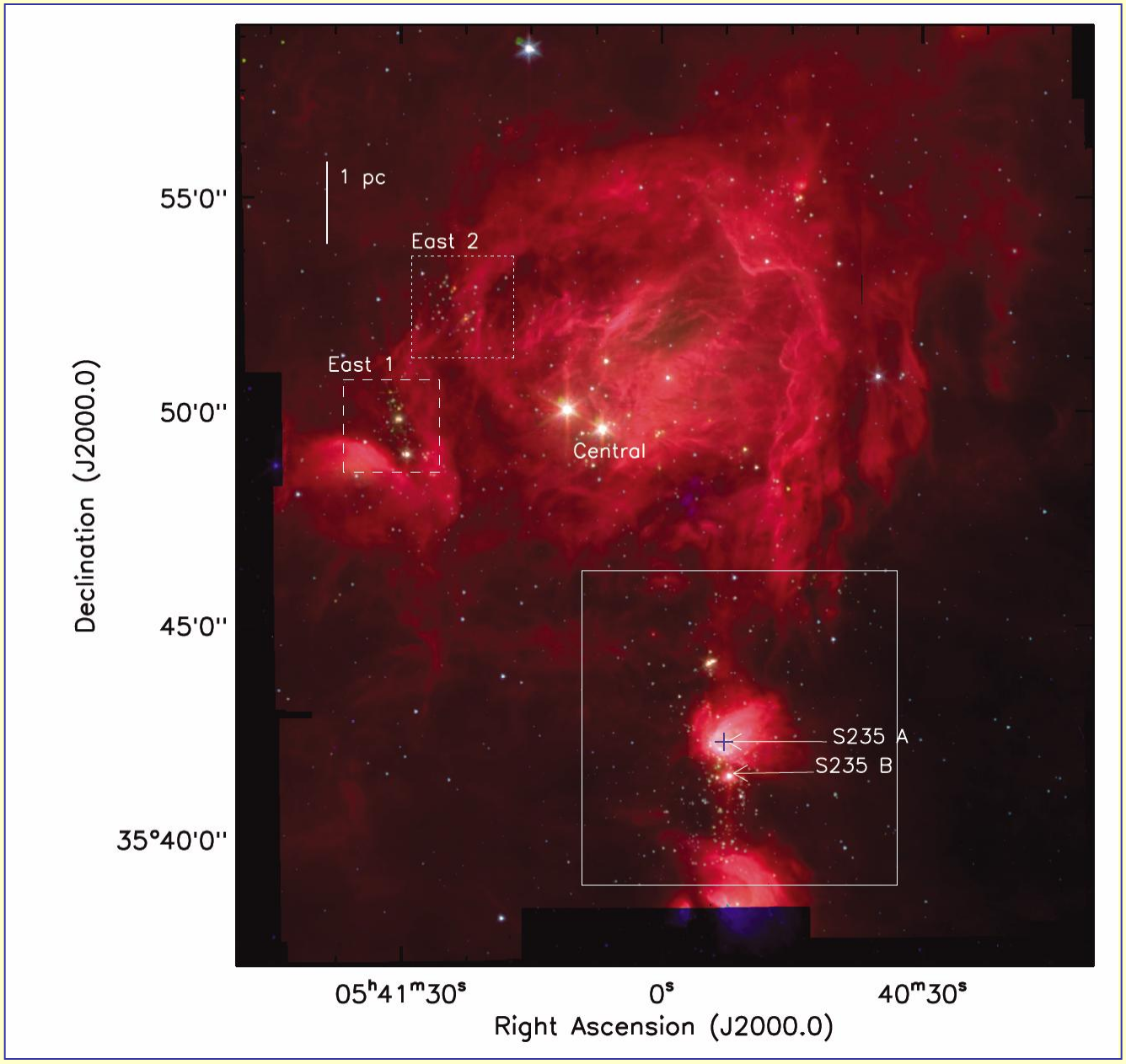

S235 – Star Forming Region

Dewanagan and Anandarao MNRAS 2011

S235 – Star Forming Region

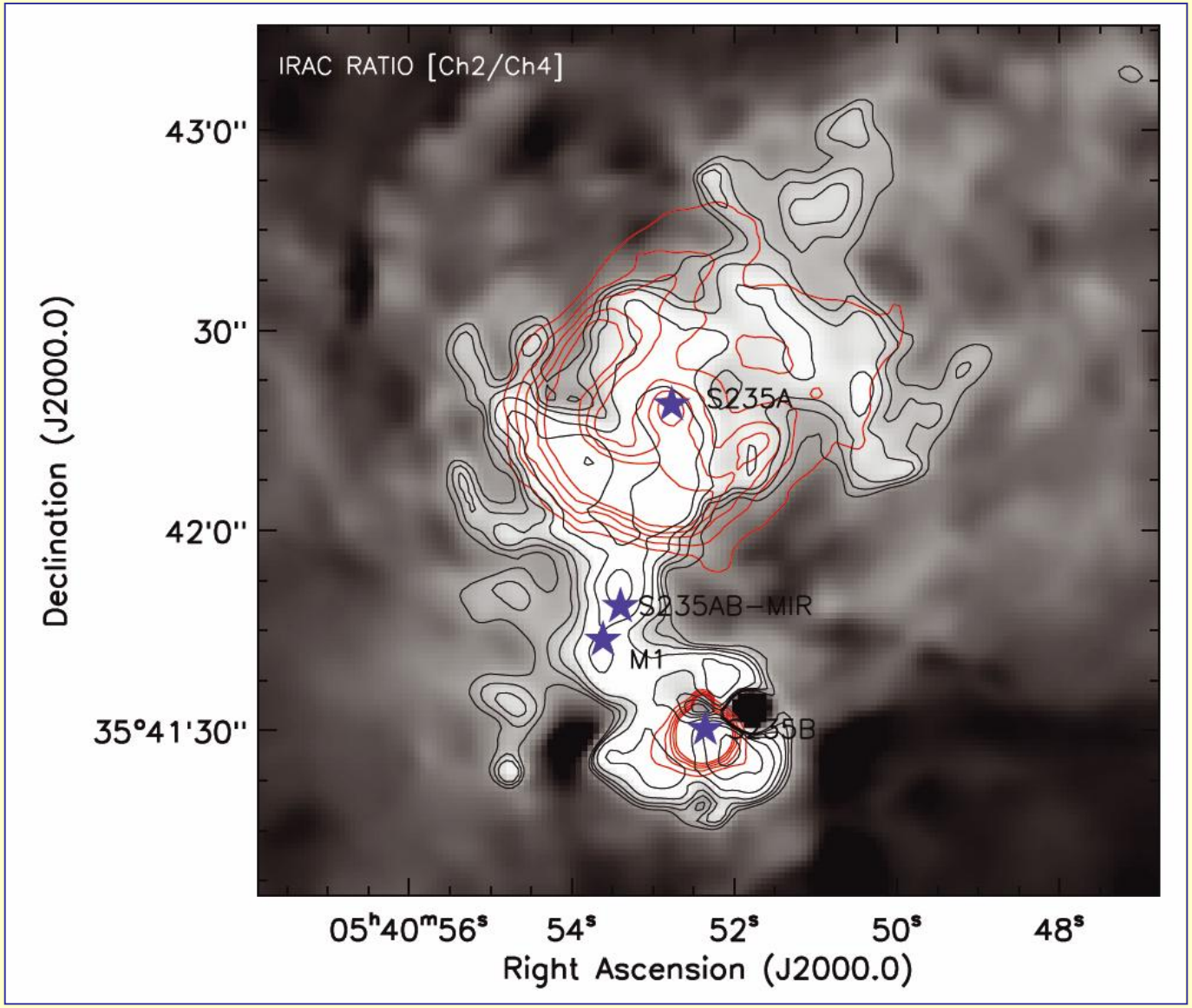

Secondary Star Formation to the South of S235A - Triggered by the expanding HII region

See the poster by Dewangan etal

Dewanagan and Anandarao MNRAS 2011

Near-Infrared Imaging Fabry-Perot Spectrometer

Molecular Hydrogen (2.121 micron) Emission in Orion showing Outflows from Young Stellar Objects (Protostars)

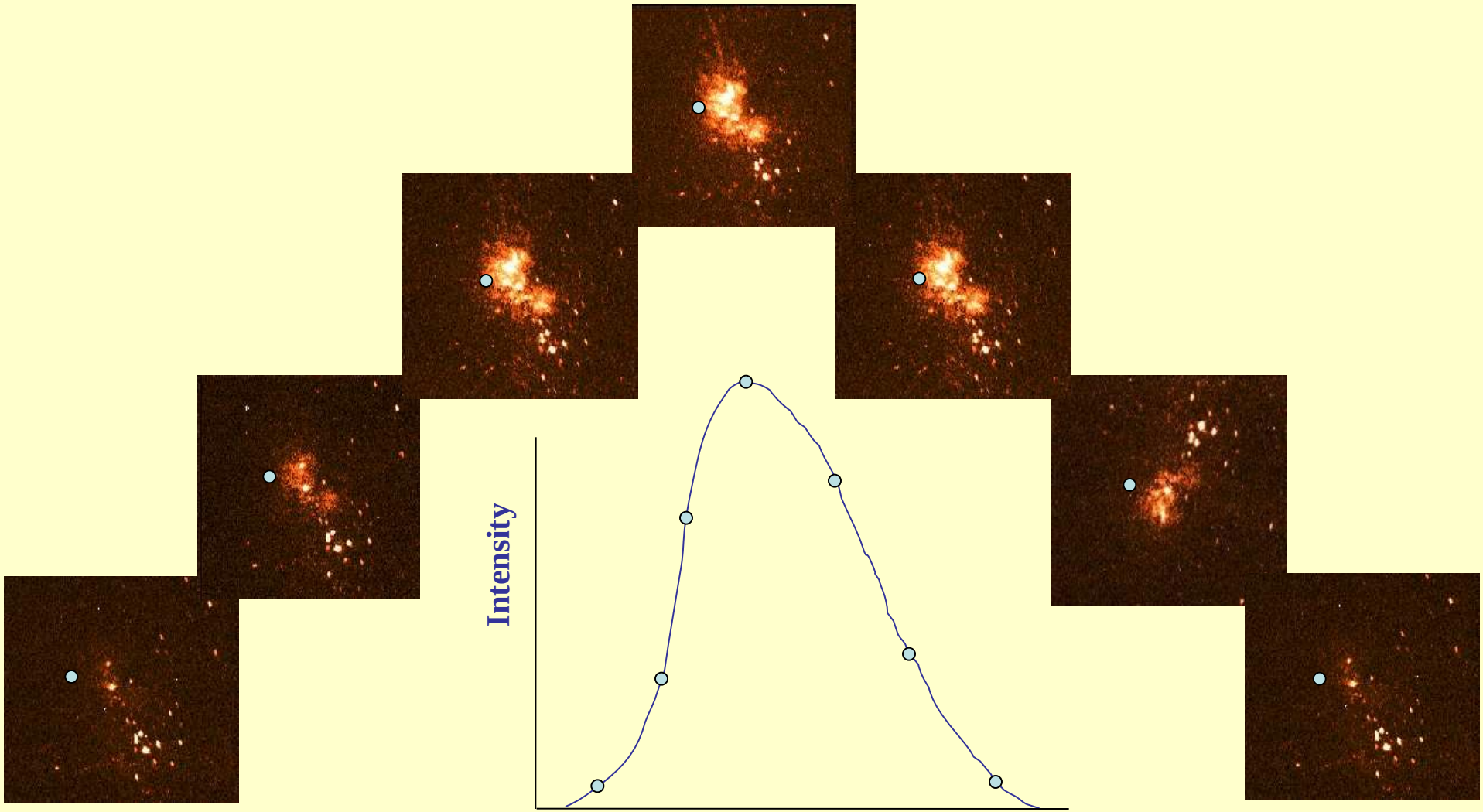

Scanning in Space and Wavelength

Wavelength or Velocity

Anandarao et al 2000, BASI

3-COLOUR IMAGE of NGC 6710

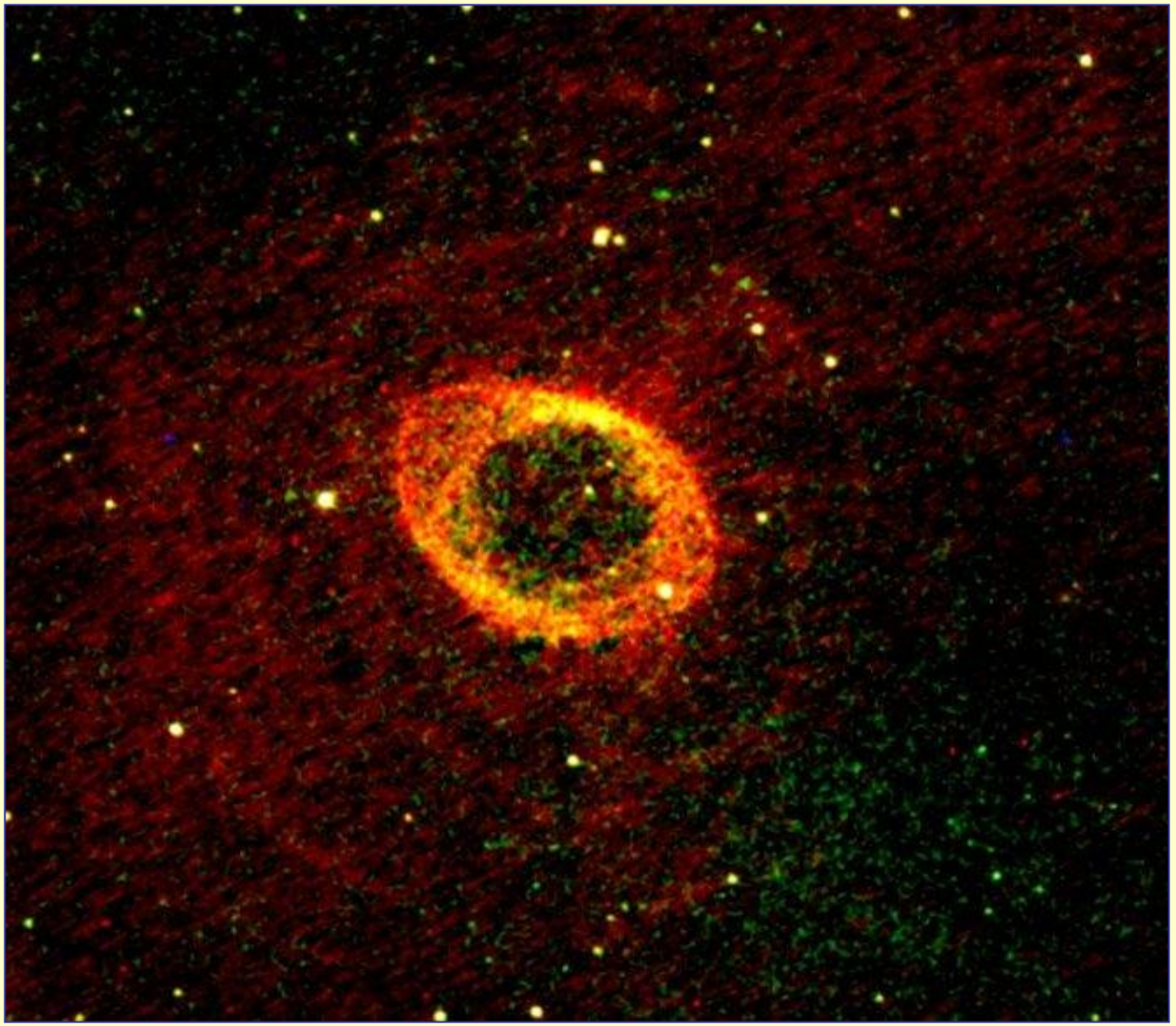

Multi-wavelength infrared image – red is molecular hydrogen; green is infrared continuum; blue is atomic hydrogen

Conclusions

Spectral features probe star forming regions and their history

Formation by accretion even for massive stars (< late O type)

Features in Debris Disks indication for future planet formation

PAH mapping indicates soft UV leaks and PDRs

Multi-wavelength observations

Fabry-Perot Imaging for accurate Ratio Mapping

Thanks for your kind attention

Contributions to ISM Radiation Field

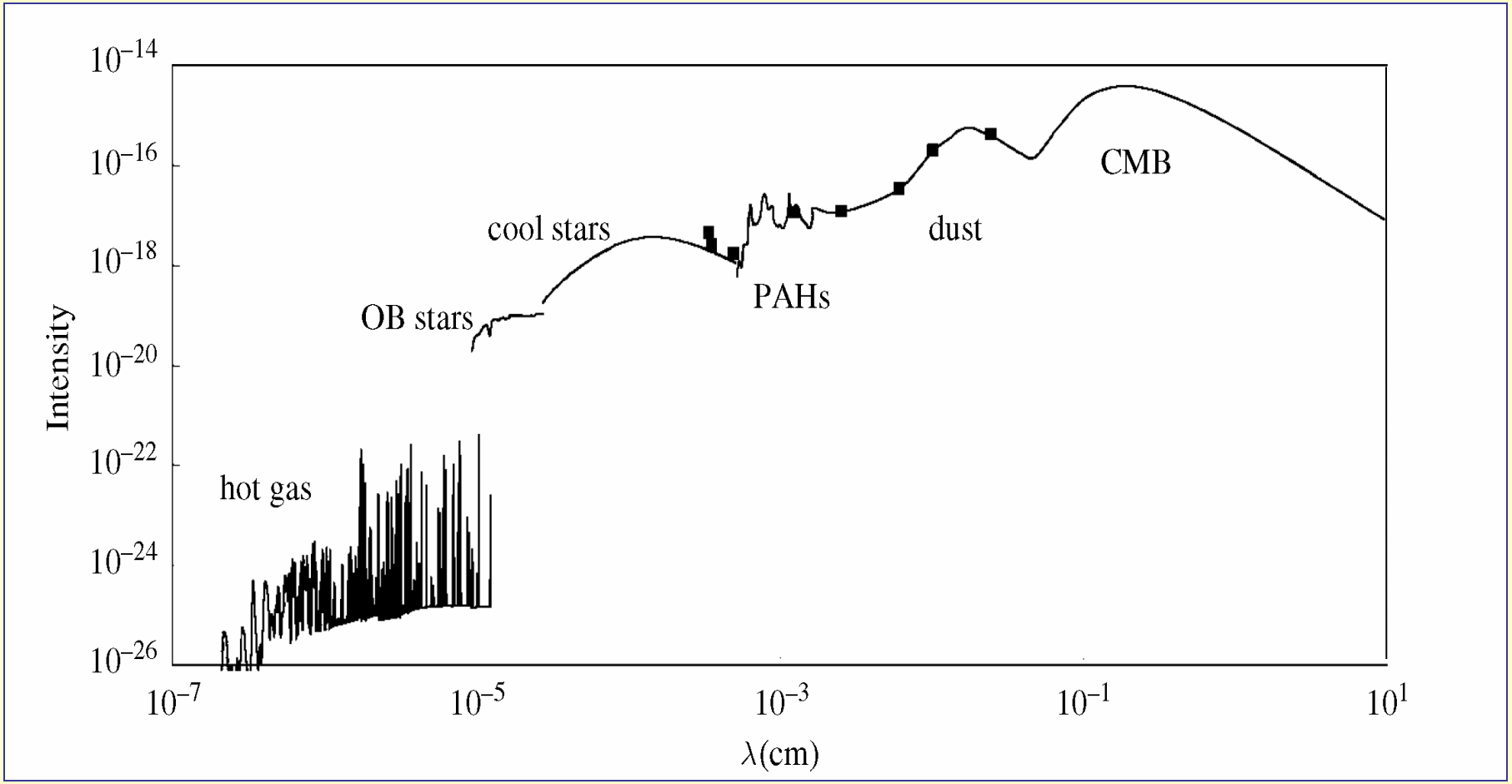

Tielens 2005

Life Cycle of Cosmic Dust

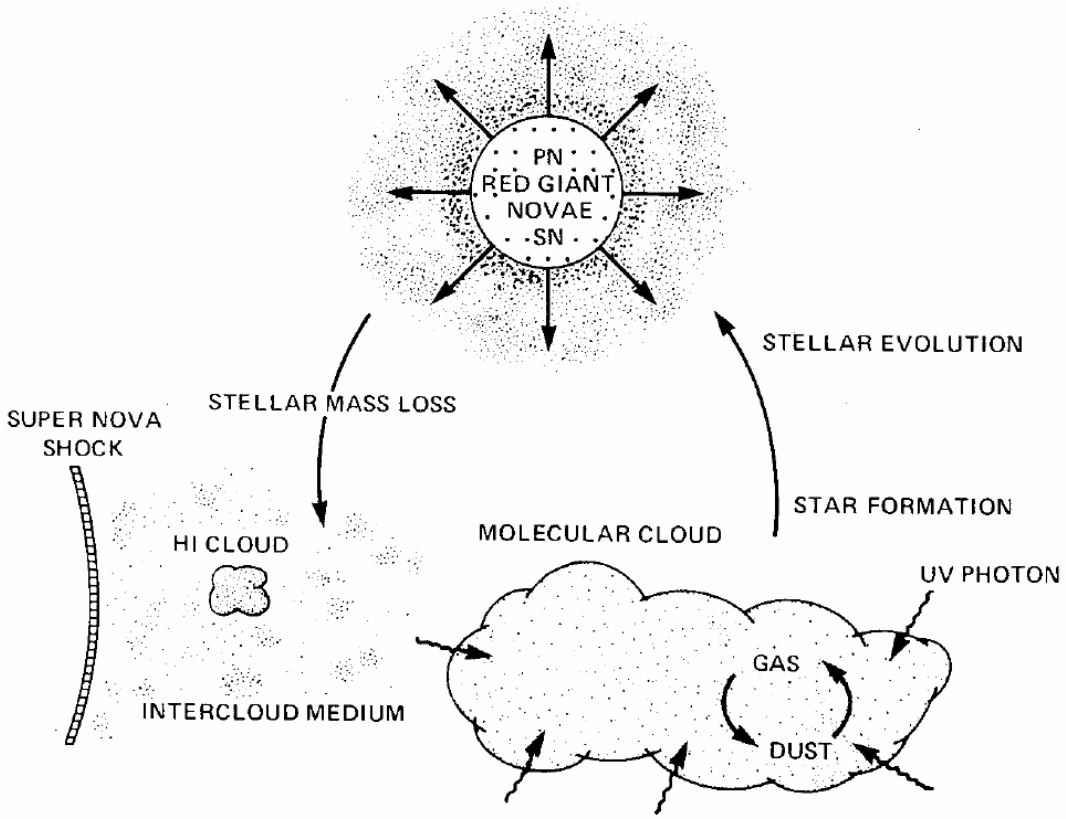

Figure 8.1. Schematic representation of the lifecycle of cosmic dust. Grains of 'stardust' originating in the atmospheres and outflows of evolved stars (red giants, planetary nebulae, novae and supernovae) are ejected into low-density phases of the interstellar medium, where they are exposed to ultraviolet irradiation and to destruction by shocks. Within molecular clouds, ambient conditions favour the growth of volatile mantles on the grains. Subsequent star formation leads to the dissipation of the molecular clouds. (From Tielens and Allamandola 1987b; reprinted by permission of Kluwer Academic Publishers.)

Astrophysical Shocks

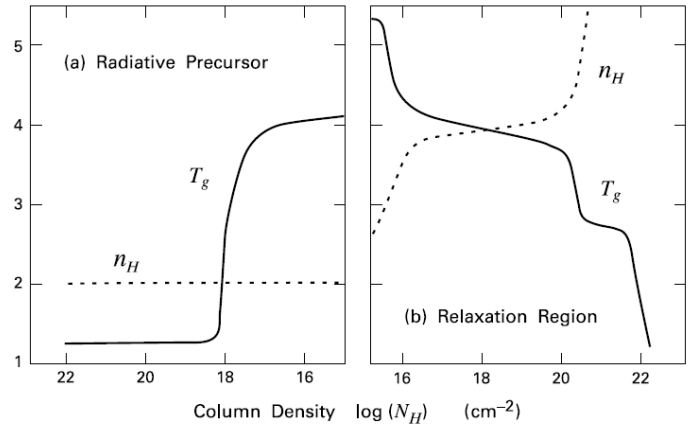

Figure 8.10 Gas temperature and hydrogen number density in a shocked molecular cloud, where $V_{\rm shock} = 80\,{\rm km\ s^{-1}}$. The graph actually displays $\log(T_g)$ and $\log(n_H) - 3$. Both quantities are shown as functions of hydrogen column density (a) upstream from the shock front, and (b) behind it. The reference frame is that for which the front is stationary.

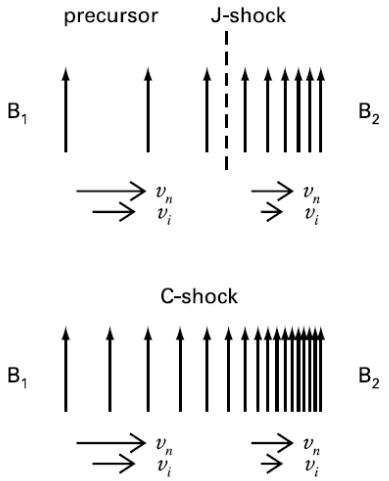

Figure 8.11 Shocks in a magnetized fluid. Depicted are the magnetic field, along with the neutral and ion velocities. Here the field is perpendicular to the flow, and the reference frame is again that in which the shock front is stationary. *Upper panel:* At low field strengths, the neutrals undergo a J-shock after crossing the magnetic precursor. *Lower panel:* For stronger fields, the neutral velocity declines smoothly. In all cases, both the field strength and ion speed change smoothly. The net change in the field is always governed by equation (8.56) in the text.

gas temperature T_g is increased by the radiation emitted just downstream from the front. The warmed preshock region is known as the *radiative precursor*. The front itself is the transition layer in which the actual thermalization of motion occurs through collisions between the pre- and postshock atoms and molecules.[3] The thickness of this layer is roughly one particle mean-free-path in the postshock gas. For the example shown in the figure, the relevant mean-free-path pertains to collisions between ions and electrons, and is 4×10^{10} cm. This distance is so small compared to the length scale for variations outside the front that the fluid essentially undergoes a discontinuous change in its properties. The temperature, density, and pressure while the velocity is reduced to a value that is subsonic with respect to the local Downstream from the front, the gas temperature falls, first quickly and then more extended *relaxation region* (Figure 8.10b). It is the radiation generated in this coo has provided our knowledge of shocks in star-forming environments.

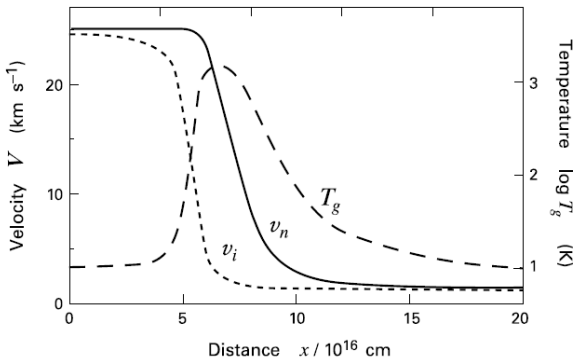

Figure 8.12 Structure of a C-shock in a molecular cloud. Here, $V_{\rm shock} = 25\,{\rm km\ s^{-1}}$, $n_H = 10^4\,{\rm cm^{-3}}$, and $B = 100\,\mu{\rm G}$, where n_H and B refer to the preshocked state. Displayed are the gas temperature T_g, the neutral velocity v_n, and the ion velocity v_i. The shock is stationary in the adopted reference frame.

Stahler & Palla 2004